UPGRADE OF PIXEL SENSOR TELESCOPE FOR CHARACTERIZATION OF ALPIDE SENSOR

Jetnipit Kaewjai

A Thesis Submitted in Partial Fulfillment of the Requirements for the

Degree of Master of Science in Physics

Suranaree University of Technology

Academic Year 2019

การปรับปรุงพิกเซลเซนเซอร์เทเลสโคปสำหรับการศึกษาคุณสมบัติอัลไพด์เซนเซอร์
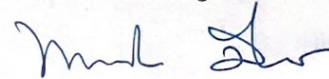
นายเจตนิพิฐ แก้วใจ

วิทยานิพนธ์นี้เป็นส่วนหนึ่งของการศึกษาตามหลักสูตรปริญญาวิทยาศาสตรมหาบัณฑิต
สาขาวิชาฟิสิกส์
มหาวิทยาลัยเทคโนโลยีสุรนารี
ปีการศึกษา 2562

UPGRADE OF PIXEL SENSOR TELESCOPE
FOR CHARACTERIZATION OF ALPIDE SENSOR
FOR HIGH ENERGY PARTICLE DETECTORS

Suranaree University of Technology has approved this thesis submitted in partial fulfillment of the requirements for a Master's Degree.
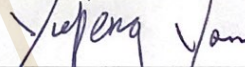
Thesis Examining Committee

_____
(Assoc. Prof. Dr. Panomsak Meemon)

Chairperson

_____
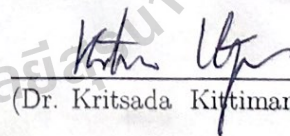(Asst. Prof. Dr. Chinorat Kobdaj)

Member (Thesis Advisor)

_____
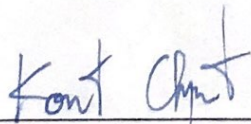(Prof. Dr. Yupeng Yan)

Member

_____
(Asst. Prof. Dr. Christoph Herold)

Member

_____
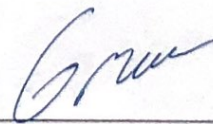(Dr. Kritsada Kittimanapun)

Member

_____
(Assoc.Prof.Flt.Lt.Dr.Kontorn Chamniprasart)

Vice Rector for Academic Affairs

and Internationalization

_____
(Assoc.Prof.Dr.Worawat Meevasana)

Dean of Institute of Science

เจตนิพิฐ แก้วใจ : การปรับปรุงพิกเซลเซนเซอร์เทเลสโคปสำหรับการศึกษาคุณสมบัติอัลไพด์
เซนเซอร์ (UPGRADE OF PIXEL SENSOR TELESCOPE FOR CHARACTERIZATION OF
ALPIDE SENSOR) อาจารย์ที่ปรึกษา : ผู้ช่วยศาสตราจารย์ ดร.ชิโนรัตน์ กอบเดช, 80 หน้า

สถานีตรวจวัดการชนอนุภาคขนาดใหญ่ หรือ อลิซเป็นสถานีทดลองที่เซิร์น ใช้สำหรับตรวจจับ
พลาสมาควาร์ก - กลูออนซึ่งเป็นสถานะของสสารที่คิดว่าก่อตัวขึ้นทันทีหลังจากเกิดบิ๊กแบง ภายหลังได้มี
การเสนอแผนเพื่อปรับปรุงเครื่องตรวจวัดอนุภาคในส่วนของระบบติดตามเส้นทางเดินของอนุภาคชั้นใน
ของอลิซภายในปี 2021 เทคโนโลยีซิลิกอนใหม่ได้ถูกนำมาพัฒนาเป็นเซนเซอร์ชนิดแมพส์และใช้ในขั้นตอน
การปรับปรุงเครื่องตรวจวัดอนุภาค ซึ่งเซนเซอร์ตัวใหม่นี้มีเรียกว่าอัลไพด์ โดยงานวิจัยนี้มุ้งเน้นที่การศึกษา
ลักษณะเฉพาะของเซนเซอร์อัลไพด์ด้วยพิกเซลเซนเซอร์เทเลสโคปรุ่นใหม่โดยใช้ลำแสงอิเล็กตรอนที่
พลังงาน 1.2 GeV ที่สถาบันวิจัยแสงซินโครตรอน โดยตัวงานต้องการที่จะศึกษาพิกเซลเซนเซอร์เทเลสโคป
รุ่นใหม่ในกรณีที่มุมของเซนเซอร์ตัวที่ทดสอบเปลี่ยนไป การจำลองการทดสอบพิกเซลเซนเซอร์เทเลสโคป
รุ่นใหม่ได้ใช้ซอร์ฟแวร์ G4beamline และข้อมูลที่เกิดขึ้นถูกเก็บไว้ในรูปแบบไฟล์ ROOT จากข้อมูลที่ได้มา
สามารถนำมาวิเคราะห์ผลซึ่งทำให้ได้แผนภาพตำแหน่งการชนของอนุภาคบนเซนเซอร์และกราฟความ
สัมพันธ์ของตำแหน่งการชน จากการวิเคราะห์ดังกล่าวสามารถนำไปทำนายมุมกระเจิงของอนุภาคได้ซึ่งมี
ค่าเท่ากับ 0.0098-0.00102 เรเดียนในกรณีที่มุมของเซนเซอร์ตัวทดสอบไม่เปลี่ยนไป นอกจากนี้ผลการ
ทำนายดังกล่าวยังถูกนำมาเปรียบเทียบและวิเคราะห์กับผลการคำนวณที่ได้จากทฤษฎี

สาขาวิชาฟิสิกส์   ลายมือชื่อนักศึกษา _____
ปีการศึกษา 2562   ลายมือชื่ออาจารย์ที่ปรึกษา _____

JETNIPIT KAEWJAI : UPGRADE OF PIXEL SENSOR TELESCOPE
FOR CHARACTERIZATION OF ALPIDE SENSOR FOR HIGH
ENERGY PARTICLE DETECTORS THESIS ADVISOR: ASST .PROF.
CHINORAT KOBDAJ, Ph.D. 80 PP.

ALICE/MONOLITHIC ACTIVE PIXEL SENSOR/ALPIDE

A Large Ion Collider Experiment (ALICE) is an experimental station at CERN that study a quark-gluon plasma, a state of matter thought to have formed immediately after the big bang. A plan was proposed to upgrade the particle detector in the Inner Tracking System (ITS) of ALICE by 2021. In the upgrade, new silicon sensor technology, the Monolithic Active Pixel Sensor (MAPS), will be used. The new sensor is called ALICE PIxel DEtector (ALPIDE). This research focused on the characterization of ALPIDE sensors with a new version of a pixel sensor telescope using the 1.2 GeV electron beam at the Synchrotron Light Research Institute Beam Test Facility (SLRI-BTF). This work focus on the study of the pixel sensor telescope in case that the angle of the Device Under Test (DUT) plane is changed. G4beamline software is used to simulate. A ROOT file is created after the G4beamline simulation finishes. The result of the analysis performs the beam profile, correlation plot. Those results were used to predict the scattering angle which is equal to 0.0098-0.00102 rad in DUT not rotated case. Moreover, the analysis result was compared with the calculation from the theory.

School of Physics	Student's Signature _J. Kaewjai_
Academic Year 2019	Advisor's Signature _C. Kobdaj_

ACKNOWLEDGEMENTS

CONTENTS

CONTENTS (Continued)

CONTENTS (Continued)

LIST OF TABLES

LIST OF FIGURES

LIST OF FIGURES (Continued)

LIST OF FIGURES (Continued)

LIST OF FIGURES (Continued)

Figure   **Page**

LIST OF FIGURES (Continued)

LIST OF ABBREVIATIONS

ALICE	A Large Ion Collider Experimental
ALPIDE	ALICE Pixel Detector
ASIC	Application Specific Integrated Circuits
BH	Bending Magnet Horizontal
BTF	Beam Test Facility
BV	Bending Magnet Vertical
DAC	Digital to Analog Converter
DAQ	Data acquisition
DUT	Device Under Test
EMCal	Electromagnetic Calorimeter
FIFO	First-In First-Out
HBT	High-energy Beam Transport line
HFT	Heavy Flavor Tracker
HMPID	High Momentum Particle Identification
ITS	Inner Tracking System
QGP	Quark-Gluon Plasma
MAPS	Monolithic Active Pixel Sensor
LBT	Low-energy Beam Transport line
LS2	2nd Long Shutdown
MIPs	Minimum Ionizing particles

LIST OF ABBREVIATIONS (Continued)

PID   Particle Identification

PHOS   Photon Spectrometer

QF   Quadrupole Focusing

QD   Quadrupole Defocuing

RHIC   Relativistic Heavy Ion Collider

RICH   Ring Imaging Cherenkov

SDD   Silicon Drift Detectors

SLRI   Synchrotron Light Research Institute

SPD   Silicon Pixel Detectors

SRAM   Static Random-Access Memory

SSD   Silicon Strip Detectors

STAR   Solenoidal Tracker

TOF   Time-Of-Flight

TPC   Time Projection Chamber

CHAPTER I

INTRODUCTION

Large Hadron Collider (LHC) at the European Organization for Nuclear Research (CERN) is currently the largest particle accelerator in the world. It has been in operation since the 10th September 2008. There are four large experiments around the LHC ring, which are A Toroidal LHC ApparatuS (ATLAS), Compact Muon Solenoid (CMS), A Large Ion Collider Experiment (ALICE), and Large Hadron Collider beauty (LHCb). LHC aims to allow physicists to test the many theories of particle physics on new particles, and to study other unsolved questions.

ALICE, one of the four experiment, is especially designed to study the physics of strongly interacting nuclear matter and the properties of the Quark-Gluon Plasma (QGP) (Satz, 2011). For the second long shut down (LS2) of the LHC, the ALICE collaboration has been preparing a major upgrade of its apparatus to improve measurement precision, and the event readout rate. One of the main upgrades is a new Inner Tracking System (ITS), in which the Monolithic Active Pixel Sensor (MAPS) (Mager, 2016) is being used as the key of the upgrade. It is an image sensor that integrates both the readout electronic and silicon parts on a single sensor unit.

1.1 The Quark-Gluon Plasma (QGP)

Quantum chromodynamics (QCD) is the theory of strong interaction. It describes the fundamental interaction between quarks and gluons which are main components of matters (Ranjan and Ravishankar, 2010). In the quark matter phase diagram, QGP is placed in the high-temperature, high-density. QGP can be studied by phase diagram in figure 1.1 as a function of temperature T and baryon number chemical potential μ.
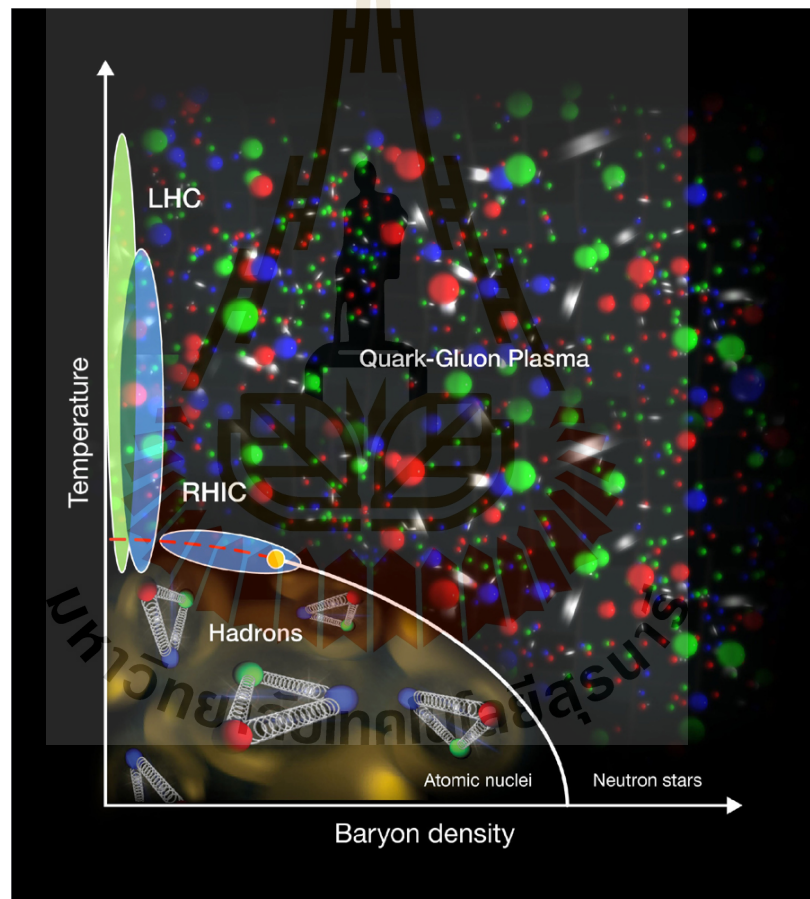
Figure 1.1 The phase diagram of quantum chromodynamic (Ranjan and Ravishankar, 2010).

1.2 A Large Ion Collider Experiment

The ALICE experiment provides a comprehensive study of electrons, photons, muons, hadrons, and jets that are created in heavy-ion collisions (Moore and Teaney, 2005). The precision of measurements complements the heavy-ion that is accelerated by using p–p and p–Pb to produce a quantitative base for comparison with results from Pb–Pb collisions.

The nature of QGP is an almost ideal liquid emerged from the experiment. The ALICE experiment has provided the basic knowledge of QGP. They observe the creation of the hadronic matter at unprecedented values of temperatures and energy density. The precision and accuracy of all significant probes are reached. ALICE has achieved these physics results after three years of the Pb–Pb and two years of the p–Pb running, respectively. ALICE has shown excellent capabilities that measure the high-energy nuclear collisions at the LHC.

The ALICE apparatus (see figure 1.2) consists of a central barrel. This component is a part used to measure hadrons, electrons and photons. The central barrel covers polar angles from 45° to 135°. It is implanted in a large solenoid magnet. Moving from centre to periphery, it consists of several detectors: the already mentioned Inner Tracking System (ITS) that will be described in the next section, a cylindrical Time-Projection Chamber (TPC), Time-of-Flight (TOF), Ring Imaging Cherenkov (RIC), and Transition Radiation (TRD) detectors, and two electromagnetic calorimeters (PHOS and EMCAL). All detectors cover the full azimuth, without these components (HMPID, PHOS, and EM-CAL). The forward muon arm (2° - 9°) consists of a complex system of absorbers. They are composed of three components, a large dipole magnet, fourteen planes of tracking,
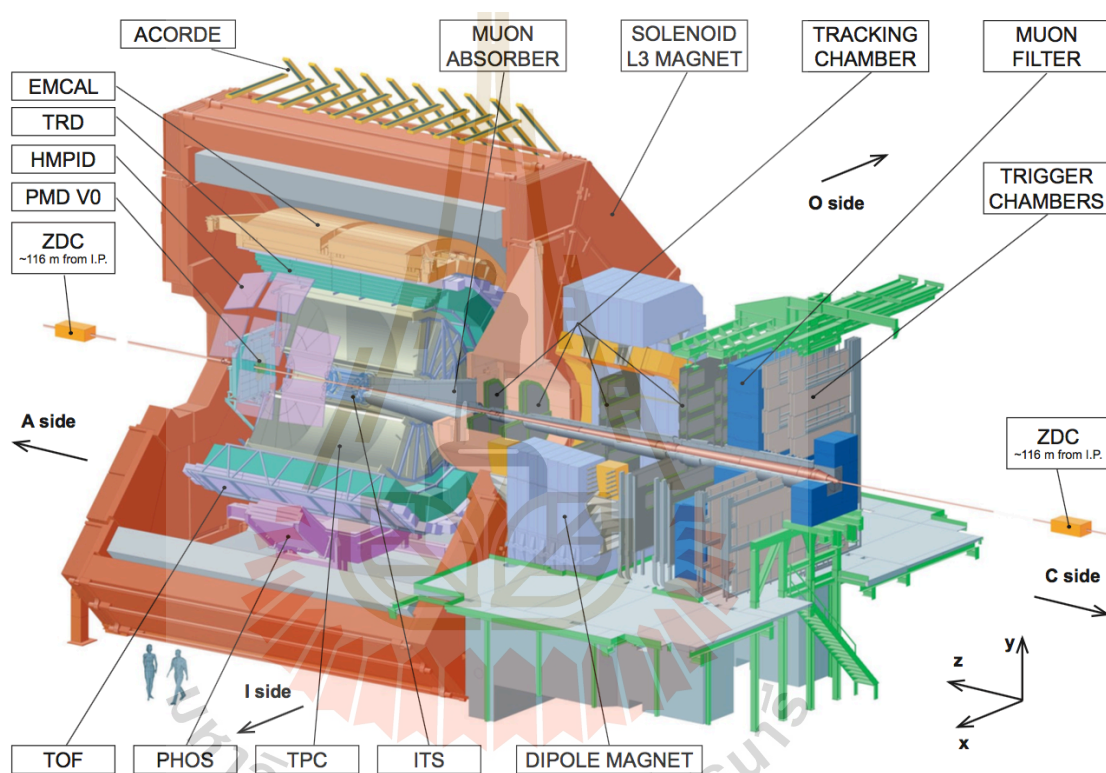
Figure 1.2 The layout of the components of ALICE detector. (Aamodt et al., 2008).

and triggering chambers. Several smaller detectors (ZDC, PMD, FMD, T0, V0) for global event characterization and triggering are located at very small angles. An array of scintillators (ACORDE) on top of the L3 magnet is used to trigger on cosmic rays.

1.3   ALICE Inner Tracking System upgrade

1.3.1   The motivation of ALICE experiment

Strong nuclear force can be studied by the interactions within the nuclei. In general, the nuclei consists of two main types of particles, neutrons and protons. Neutrons and protons are made of up and down quarks. Since their masses are very low, we can study them in a low-energy accelerator. This is contrary to the study of strange and charm quarks. Since their masses are higher and cannot be found in nature, we have to use a high-energy accelerator as a tool.

To understand the strong nuclear force and the properties of strange and charm quarks more, we aim to study the formation of hypertriton and Λ_C particles. In the past, it was difficult because these two particles have high masses with low transverse momentum and lose energy easily when moving through medium. It is expected that after improvement of the ALICE components, the ITS will be able to provide more information on the process of lambda particle generation. Table 1.1 shows the performance improvement of the upgraded ITS comparing to the present ITS. The detector can detect high mass particles such as Λ_C and D mesons at low transverse momentum.

Table 1.1 Comparison between the present and upgraded ITS.

Observable	Current, 0.1 nb^{-1}	Upgrade, 10 nb^{-1}
D meson R_{AA}	$p_T > 1$, 10%	$p_T > 0$, 0.3%
D_s meson R_{AA}	$p_T > 4$, 15%	$p_T > 1$, 1%
D meson from B R_{AA}	$p_T > 1$, 50%	$p_T > 0$, 2.5%
D meson elliptic flow (for $v_2 = 0.2$)	$p_T > 1$, 50%	$p_T > 0$, 2.5%
D from B elliptic flow (for $v_2 = 0.1$)	not accessible	$p_T > 2$, 20%
Charm baryon/meson ratio (Λ_C/D)	not accessible	$p_T > 2$, 15%
J/Ψ R_{AA} (forward y)	$p_T > 0$, 1%	$p_T > 0$, 0.3%
J/Ψ R_AA (central y)	$p_T > 0$, 5%	$p_T > 0$, 0.5%
J/Ψ elliptic/flow (forward y, for $v_2 = 0.1$)	$p_T > 0$, 15%	$p_T > 0$, 5%
Ψ	$p_T > 0$, 30%	$p_T > 0$, 10%
Temperature IMR	not accessible	20% on T
Elliptic flow IMR (for $v_2 = 0.1$)	not accessible	20%
Low-mass vector spectral function	not accessible	$p_T > 0.3$, 20%

1.3.2 ALICE upgrade plan

ALICE already proved to provide a very good performance for detecting particles in heavy ion collisions. It confirmed the basic picture of the nature of QGP. The ALICE long-term physics goals are discussed in detail in the ALICE Upgrade Letter of Intent, Conceptual Design Report (CDR) (Musa, 2012) and Technical Design Report (TDR) (Abelev et al., 2014). Topics to be addressed include heavy-flavor hadrons, quarkonia, and low-mass dileptons. The upgrade of the detector element can found those particles at low transverse momenta. The improvement is also an increase in statistics. The capability to study these processes will be greatly enhanced. ALICE has been developing a major upgrade of the new ITS, and a plan for installation during the Long Shutdown 2 (LS2) of the LHC in 2019/20 (Keil, 2015) (see in figure 1.3) by:

- Development of elaborate parameters measurement of collision

  - Reduction of the first detection layer closer to the beam pipe to reduce the distance from beampipe to the first layer (<22 mm)

  - Reduction of material budget of inner layers from 1.14% to 0.30%

  - Reduction of sensor's size and thickness by using Monolithic Active Pixel Sensor.

- Improvement of read-out time

  The present ITS features have a maximum read-out rate of 1 kHz, while the new detector is designed to be able to read the data related to each individual interaction up to a rate of 100 kHz.

- Adjustment of detector layout

  The current ITS consists of six layers, two inner layers of Silicon Pixel Detector (SPD), two middle layers of Silicon Drift Detector(SDD), and two

outer layers of Silicon Stripe Detector (SSD). The present ITS will be fully replaced by a new detector consisting of seven layers of monolithic silicon pixel detectors. The new detector consists of two separate barrels: an inner barrel (IB) comprising of three inner layers and an outer barrel (OB) comprising of two middle and two outer layers.
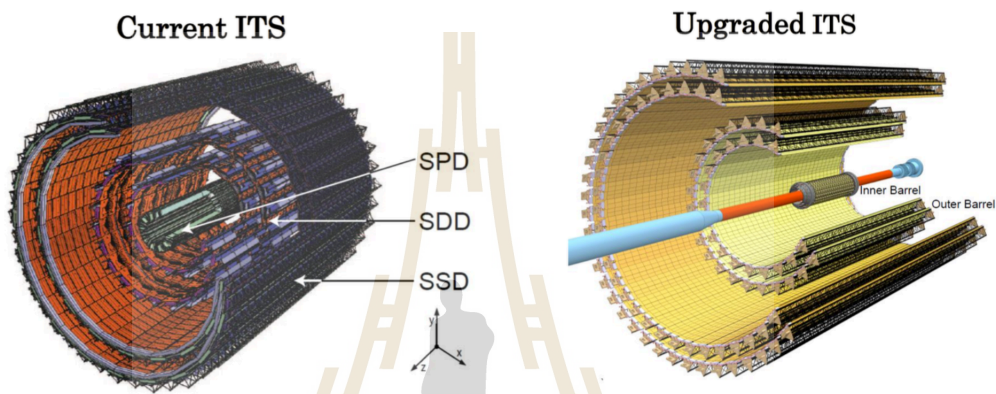
Figure 1.3 The elementary layers of present ITS (left) and upgrade ITS (right). (Aamodt et al., 2008).

1.4 Thesis outline

This thesis is structured as follows. In chapter II, the properties of silicon detector material and the principles of operation of MAPS are discussed. In chapter III, the ALICE Inner Tracking System upgrade is introduced. Within this thesis, small-scale and full-scale Monolithic Active Pixel Sensor (MAPS) prototypes for the ALICE ITS Upgrade were characterized. The structure of SLRI-BTF and the installation of a pixel sensor telescope are given in Chapter IV. The new pixel sensor telescope is presented by using trajectory prediction, and the modification sensor telescope will be built within this thesis is described in Chapter V. Moreover, the summary of the surface commissioning at CERN is also added in this

chapter. The performance of the new pixel sensor telescope based on a simulation using G4beamline software and the analysis using ROOT framework are explained in Chapter VI. The results and prospects for future at looks are shown in Chapter VII.
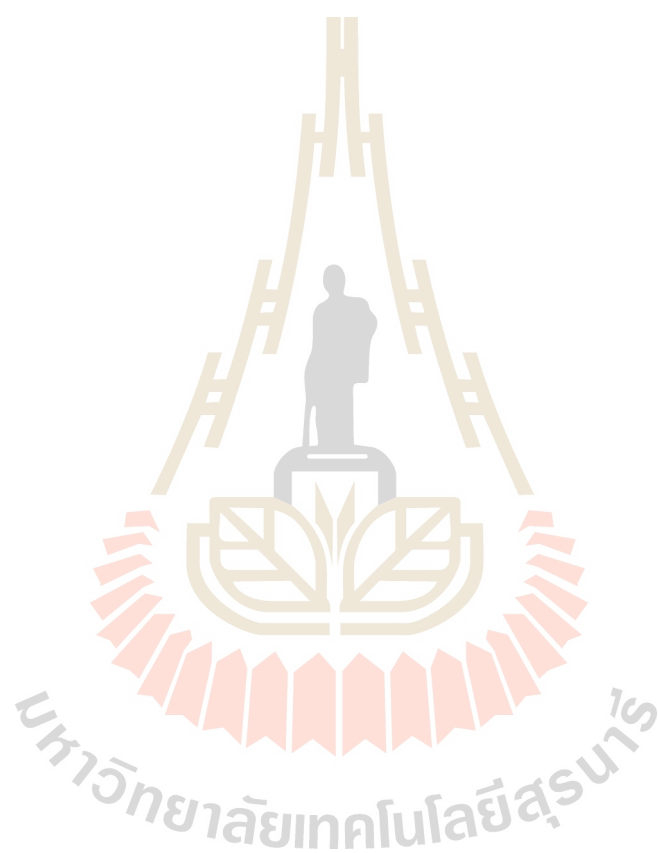
CHAPTER II

MONOLITHIC ACTIVE PIXEL SENSORS

This chapter discusses about the development of the new silicon pixel sensor technology for the new ALICE ITS, named ALPIDE. The new sensor will be implemented in the 180 nm CMOS process by TowerJazz technology. Moreover, this chapter also describes the principles of charge carriers and their collection within the sensitive layer.

The first part of this chapter gives a review of the energy-loss mechanisms of charged particles and electromagnetic radiation in Silicon.

2.1 Energy deposit and charge generation in silicon

In this section, a brief overview of charge deposit mechanisms in silicon, relevant for this work, is provided.

2.1.1 Energy loss of charged particles

Charged particles are positrons and electrons. The large difference in mass between electrons and heavy charged particles has important consequences for interactions. A charged particle deposits energy through two mechanisms. The first mechanism is collisional losses, which lead to excitation of the atom or ionization. Bethe-Bloch formula gives the mean rate of energy loss (stopping power) (Morgan Jr and Eby, 1973) for a heavy charged particle (eq 2.1). The second mechanism is radiative losses. The energy loss is slightly different because of their small masses and indistinguishability properties (requiring relativistic term). Fast

charged particles moving through matter interact with the electrons of atoms in the material. The interaction excites or ionizes the atoms, leading to an energy loss of the traveling particle.

$$-\frac{dE}{dx} = 4\pi N_A r_e^2 m_e c^2 z^2 \frac{Z}{A}\frac{1}{\beta^2}\left[\frac{1}{2}ln\frac{2m_ec^2\beta^2\gamma^2 T_{max}}{I^2} - \beta^2 - \frac{\delta}{2}\right] \qquad (2.1)$$

with r_e is the classical electron radius, m_e is the electron mass, N_A is the Avogadro's number, I is mean excitation potential, Z is the atomic number of absorbing material, A is the atomic weight of absorbing material, β is v/c of the incident particle, δ is density correction, T_{max} is the maximum kinetic energy which can be imparted to a free electron in a single collision, and z is particle charge.

2.1.2 Energy loss of electromagnetic radiation

The most important processes that photons undergo, when interacting with matter are the photoelectric effect, Compton (incoherent) scattering is the scattering of a photon by a charged particle (Williams, 1977). It can be explained by eq 2.2, a relationship between the shift in wavelength and the scattering angle of the X-rays by assuming that each scattered X-ray photon interacted with only one electron. λ is the initial wavelength, λ' is the wavelength after scattering, h is the Planck constant, m_e is the electron rest mass, c is the speed of light, and θ is the scattering angle.

$$\lambda' - \lambda = \frac{h}{m_e c}(1 - cos\theta) \qquad (2.2)$$

The another one is a pair production. It is the creation of a subatomic particle and its antiparticle from a neutral boson.

2.2 Radiation damage

Two radiation damage mechanisms affect semiconductor detectors:

- Non-ionising damage: Incident radiation displaces silicon atoms from their lattice sites. The resulting defects alter the electrical characteristics of the crystal.

- Ionising damage: Energy absorbed by ionization in insulating layers, usually SiO_2, liberates charge carriers, which diffuse or drift to other locations where they are trapped. This leads to unintended concentrations of charge and, as a consequence, parasitic electric fields.

2.2.1 Non-ionising radiation damage

Non-ionising radiation damage is linked to Non-Ionising Energy Loss (NIEL) (Lazanu et al., 1997) which depends on the particle type and energy. NIEL is usually expressed as equivalent fluence of 1 MeV neutrons per square centimetre (1 MeV n_{eq} cm^2).

2.2.2 Ionising radiation damage

The basic detector is insensitive to ionization effects. In the bulk, ionizing radiation creates electrons and holes that are swept from the sensitive volume. Charge can flow freely through the external circuitry to restore equilibrium. A potential problem in case of MAPS lies in the integrated circuitry in particular MOS transistors. Positive charge build-up due to hole trapping in the oxide and at the interface shifts the gate voltage required for a given operating point.

2.3 Basic physics in sensor

Knowledge required to understand the principle of sensor is based on basic electronics and semiconductor. In this section, we give brief definitions of pn-junction, depletion region, effect of magnetic field, reverse bias, and digital analog converter.

2.3.1 PN-junction

The contact between p-type and n-type semiconductors is called pn-junction. The reversely biased pn-junction is the basic building block of silicon sensors. It builds up an electric field that collects the signal from charge particle and suppresses the leakage current, an important noise source. A pixel sensor is a reversely biased pn-diode with a highly segmented cathode or anode.

2.3.2 Depletion Region

When a pn-junction is formed, some of the free electrons in the n-region diffuse across the junction and combine with holes to form negative ions (Bakowski and Gustafsson, 1998). Filling a hole makes a negative ion and leaves behind a negative ion on the n-side. A space charge builds up, creating a depletion region which inhibits electron transfer by putting a forward bias on the junction. Diffusion is the random movement of the charge carriers that implies gradient in the carrier concentration. It is more probable that a carrier from a high-concentration region arrives at a low-concentration region. The diffusion $\mathbf{J}_{n,diff}$ is described by

$$\nabla J = -\frac{\partial \phi}{\partial t} \tag{2.3}$$

and

$$\mathbf{J}_{n,diff} = -D_n \nabla n = -\frac{kT}{e}\mu_n \nabla n \tag{2.4}$$

$$\mathbf{J}_{p,diff} = -D_p \nabla p = -\frac{kT}{e}\mu_p \nabla p \tag{2.5}$$

where ∇n and ∇p are the gradients of the electron and hole concentration. The diffusion constants $D_{n,p}$ are related to the mobilities via the Einstein equation $D_{n,p}/\mu_{n,p} = kT$ with k is Boltzmann's constant, $\mu_{n,p}$ is the mobility of neutron and proton, and T is absolute temperature.

2.3.3 Effect of Magnetic Field

Semiconductor detectors can be operated inside a magnetic field. The magnetic field controls the drift of the signal charge and the properties of the sensor. An electron or a hole moving in an electric field is presented in the Lorentz force $\mathbf{F} = \pm e\,(\mathbf{E} + \mathbf{v} \times \mathbf{B})$. The drift direction will differ from the direction of the electric field by the Lorentz angle θ_L follow by

$$\tan\theta_{L,n} = \mu_{Hall,n}B_\perp xs \tag{2.6}$$

$$\tan\theta_{L,p} = \mu_{Hall,p}B_\perp \tag{2.7}$$

with $B_\perp$ being the magnetic field perpendicular to the drift velocity. The Hall mobility μ_{Hall} differs from the drift mobility.

2.3.4 Reverse Bias

External voltage applied in the same direction as the built-in voltage will remove noise and will extend the space charge region (depletion region). The width of the depletion zone, the electric field, and the potential as function of the

applied voltage can be calculated by solving the Poisson equation,

$$W = x_n + x_p = \sqrt{\frac{2\epsilon_0 \epsilon_{Si}}{e}\left(\frac{1}{N_A} + \frac{1}{N_D}\right)(V + V_{bi})} \tag{2.8}$$

where W is the total width of the depletion zone, x_n and x_p are paths on the n- and p-side respectively, ϵ_0 is the permitivity in vacuum, ϵ_{Si} is the permitivity of silicon, N_A is the number of ionized donors, N_D is the number of ionized acceptors, V_{bi} is the built-in voltage, and V the externally applied voltage.

2.3.5 Coulomb scattering of particles in matter

When particles pass through matter, in addition to inelastic collisions with the atomic electrons (see in figure 2.1), they have a probability to suffer from repeated elastic Coulomb scattering from nuclei.

Figure 2.1 Layout of multiple scattering of charged particles.

1. Single scattering

When the thickness of medium is very small, the probability to havemore than one interaction is negligible. The Rutherford formula describes this situation

well (Tsai, 1974),

$$\frac{d\sigma}{d\Omega} = (\frac{1}{4\pi\epsilon_0})^2 \frac{Z^2 e^4}{M^2 c^4 \beta^4} \frac{1}{sin^4(\theta/2)} \tag{2.9}$$

where M is a dimensionless quantity giving the mean number of collisions which occur in the multiple scattering process and $c\beta$ is the velocity of electron.

2. Plural scattering

When the number of Coulomb scattering increases but remains under few tens of interactions, there are different approaches to deal with these situations (Meroli, 2015).

3. Multiple scattering

When the thickness increases and the number of interactions become higher than ten, the angular dispersion can be written as Gaussian. Referring to multiple scattering, that is the most common situation, naming θ the solid angle that is concentrated the 98% of the beam after a thickness x of material, if we define $\theta_0 = \theta/\sqrt{2}$ as the projection of θ on an incidence plane, the angular dispersion can be calculated by the relation :

$$\theta_0 = \frac{13.6}{\beta cp} z \sqrt{x/X_0}[1 + 0.038\ln(x/X_0)] \tag{2.10}$$

where p is the momentum and X_0 is the radiation length. This last quantity is the characteristic of the material and can be expressed by the approximated formula

$$X_0 = \frac{716.4A}{Z(Z+1)\ln(287/\sqrt{Z})} \tag{2.11}$$

where Z is atomic number of scatterer and A is atomic weight.

2.4 Principles of MAPS operation

A typical MAPS developed for high-energy physics experiments consists of three layers (see in figure 2.2): a highly p-doped (p_{++}) substrate being mechanical support, a thin (few tens of μm) p^- epitaxial layer used as sensitive volume, and n-type and p-type implants on top of the epitaxial layer called wells. N-type implants act as collecting diodes for electrons while p-wells host the circuitry. On top of the implants, there are metal layers forming the in-pixel circuitry, and propagating the signal and bias from the chip periphery. Most of the modern MAPS are produced on high-resistivity ($\rho > 1$ kΩcm) epitaxial layer. The MAPS composition (Cavicchioli et al., 2014) is comprised of:
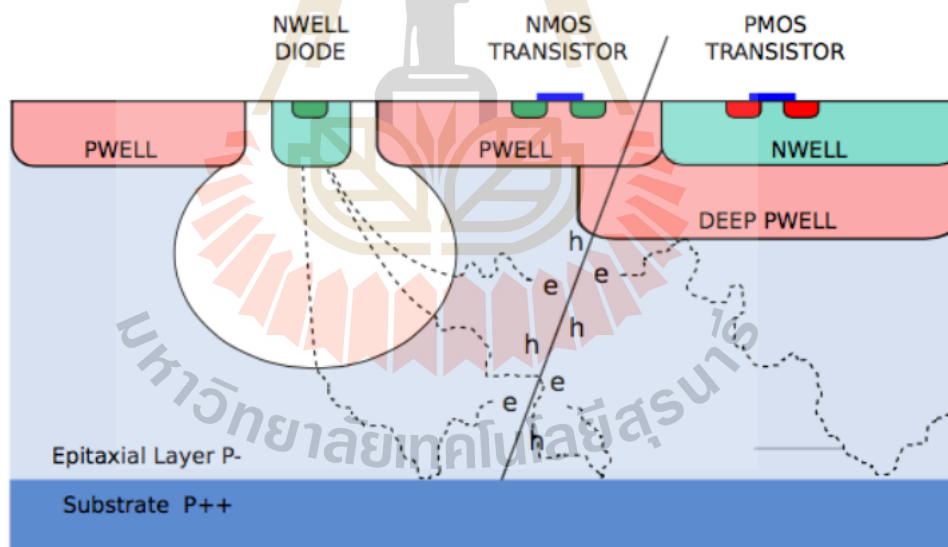
Figure 2.2 Schematic cross section of a MAPS pixel. (Aamodt et al., 2008).

- (i) A SiO$_2$ layer is a top layer of the sensor. It is the location where the electronic circuit of CMOS, such as gates and drains as well as a passivation layer to protect the surface of the sensor, are fabricated.

- (ii) An epitaxial layer is a middle layer of the sensor. By applying a reverse bias to the n-well diode on top of the epitaxial layer, a depletion region is created inside the epitaxial layer under to the n-well diode. If there are high energy particles traveling through the sensor, electron-hole pairs will be created. These generated electrons are then moved and collected at the n-well diode by a thermal diffusion process.

- (iii) The substrate is a highly p-doped (P++) silicon layer at the bottom of the sensor. At the junction of P- epitaxial and P++ layers, electrons are reflected by the built-in voltage back to the n-well collection diode.
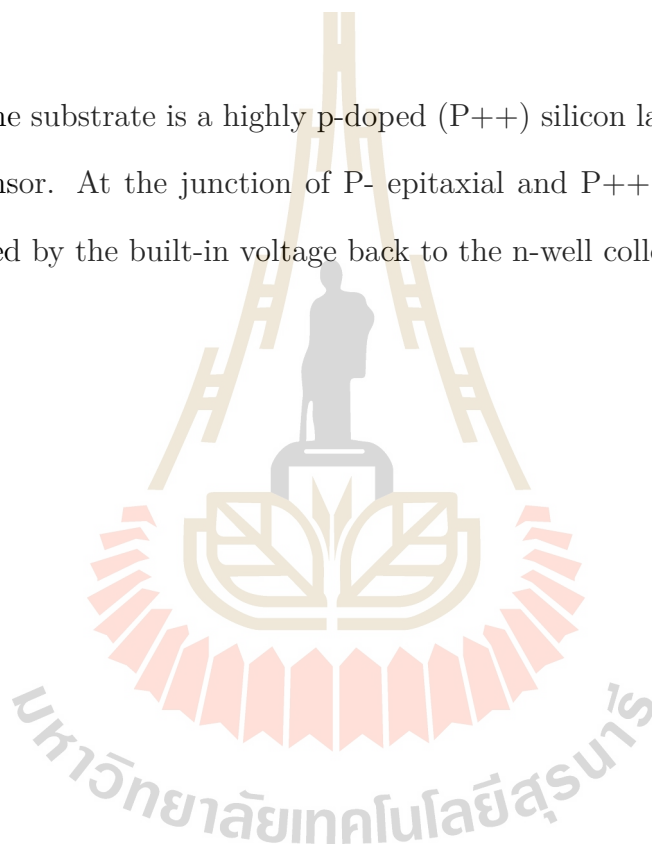
CHAPTER III

ALICE INNER TRACKING SYSTEM

UPGRADE

3.1 ALPIDE architecture

The sensor developed for the ALICE ITS upgrade is called ALPIDE, which stands for ALICE PIxel DEtector. The first prototype of this chip was fabricated in 2012. In Figure. 3.1, the development timeline of the ALPIDE chip can be seen with the main characteristics and the main purpose of each chip (Dorokhov et al., 2011). These prototypes are discussed in details in the following.

3.1.1 Small-scale prototype

There are two types of small-scale prototypes of the ALPIDE family: the Explorer and the pALPIDEss. The Explorer has an analog output, while the pALPIDEss has a digital readout.

Explorer

The Explorer was the first prototype of the ALPIDE family to optimize the sensor and the collection diode of the pixel. This prototype has two variants, Explorer-0 and Explorer-1. Explorer-0 has pixels of a size of 20 μm × 20 μm and Explorer-1 has pixels of a size of 30 μm × 30 μm. Both prototypes contain two matrices. Each of these matrices is subdivided into nine sectors with different collection diode geometries and different spacings between the collection diode and the surrounding p-well. This spacing is an area between the n-type collection

The ALPIDE family prototypes and their goals

▸ Time, Prototype : Purpose and specification

July 2012, Explorer-0

- Radiation hardness

- Reverse substrate bias

- Collection-electrode geometry and pixel

- Analogue read-out

Mar 2013, Explorer-1

- Epitaxial-layer properties

pALPIDEss-0

- Verification in matrix specification

- Front-end circuit verification

- First variant of ALPIDE architecture

Jan 2014, Investigator-0

- Charge-collection time measurement

- Pixel-pitch and electrode geometry

- 135 mini matrices

- Parallel analogue output

pALPIDEss-1

- Front-end optimization and variations

pALPIDE-1

- On-chip bias DACs

- Pads over matrix

Jan 2014, pALPIDE-2

- Final interface except high-speed link

- Epitaxial-layer properties

Jan 2015, pALPIDE-3

- High-speed link

- Three in-pixel hit buffer per pixel

Sep 2016, ALPIDE

- Containing a matrix of 512x1024 pixels

- A periphery circuit including the readout and control

Figure 3.1 The development timeline of the ALPIDE family prototypes. (Aamodt et al., 2008).

diode and the surrounding p-well (p-type), which is not doped, and it plays an important role in the shaping of the depleted volume (see in Figure 3.2).
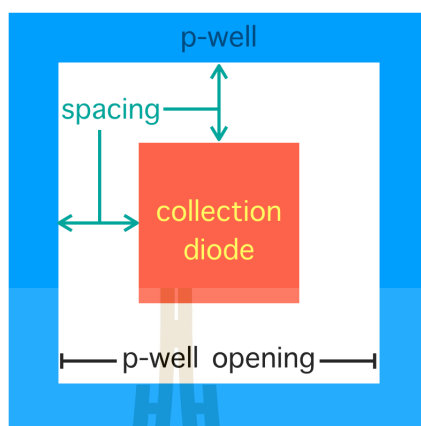
Figure 3.2 Illustration of the spacing between the collection diode and the surround- ing p-well. (Aamodt et al., 2008).

pALPIDEss

The pALPIDEss was the first ALPIDE prototype that had a digital readout. The chip has 64×512 pixels of the size $22~\mu$m $\times~22~\mu$m. The chip is split into four regions along the column direction (see in figure 3.3). These regions differ in the pixel geometries or in the possibility to inject signals into the pixels. The differentiation of the hits is done by the front-end of each pixel, and the chip is read out by an Address Encoder Reset Decoder logic (AERD). The collection electrode of all pixels is made of a n-well implant and Shallow-Trench Isolation (STI) to separate the collection n-well from the surrounding p+ ring. All pixels have an opening of 5.56 μm diameter of the p+ square surrounding the collection electrode. Half of the pixels have injection capacitors which are 0.14 fF. This capacitance is small compared to the expected input node capacitance of the order of 1 fF. Only the injection capacitors in the rows 254 to 257 are connected to an analogue input pad, the other injection capacitors are connected to ground. The pixels are the same in all pALPIDEss generations and variants. There is a diode reset in a pixels

of the pALPIDEss.

In the pALPIDEss, a Dynamic Memory Cell (DMC) based on a capacitor of 80 fF is used as an in-pixel hit buffer. During reset, the capacitor is charged. The HIT signal from the front-end controls the discharging of the capacitor by using a transistor. The length of the HIT pulse hence needs to be long and high enough to discharge the capacitor below a threshold. The pALPIDEss does not feature in-pixel masking. The priority encoder is based on standard CMOS logic cells. The AERD implementation of the pALPIDEss is slightly different compared to that of the pALPIDE. In the pALPIDEss, single-column priority encoders with 512 inputs are deployed. Furthermore, an end-of-column priority encoder combines the 64 columns. The control signals of the priority encoder are directly accessible from IO-pads giving full control to the readout system.
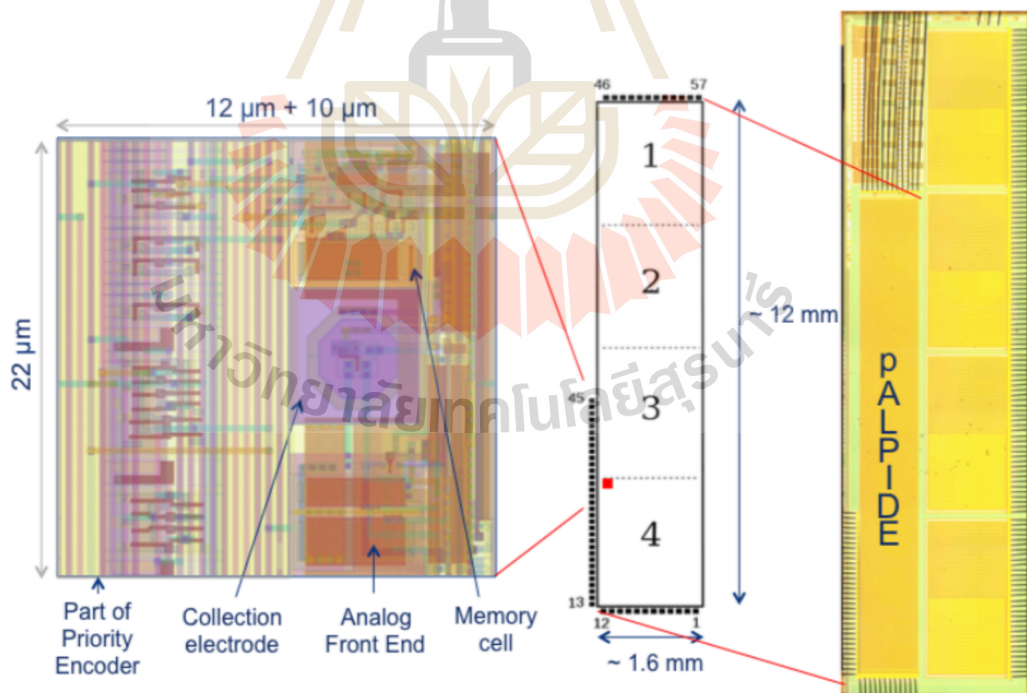
Figure 3.3 The pALPIDEss with an illustration of its division in four sectors and a layout of a single pixel. (Aamodt et al., 2008).

3.1.2 The pALPIDE-1 sensor

The pALPIDE-1 is the first large-scale prototype of the ALPIDE family, and the schematic drawing of its building blocks can be seen in figure 3.4. The pALPIDE-1 having a size of 15.3 mm × 30 mm consists of 512 × 1024 pixels, which are 28 μm × 28 μm (see in figure 3.5). The amplification and the discrimination of the analog signal are processed within each pixel, and the address of the hit pixels is encoded in the AERD similarly discussed in Sec 3.1.1 for the pALPIDEss. These addresses propagate to the periphery, where they are stored, and data-compression can be performed before transmitting the hit information of the chip. The recorded hits can be obtained from real particles passing through the sensor or noise. Analog and digital signals can be injected into selected pixels to test the response of the pixels.

The control and trigger signals are provided to the periphery, and the control logic in the periphery manages the AERD and the pixels. The bias currents and voltages are also generated in the periphery by digital to analog conversion (DAC) and propagate to all the pixels.
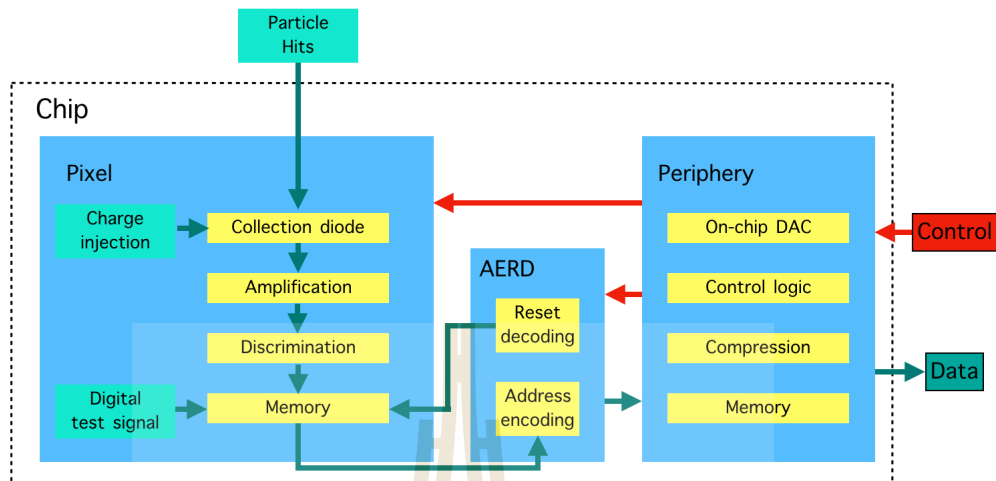
Figure 3.4 Schematic drawing of the building blocks of the digital prototypes of the ALPIDE family. (Aamodt et al., 2008).
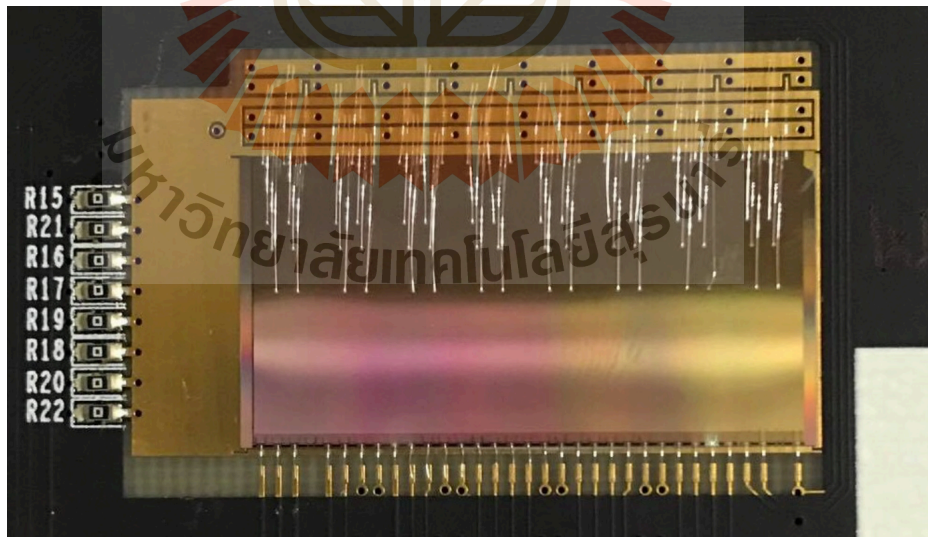
Figure 3.5 pALPIDE-1 is the first generation of the prototype ALPIDE for AL-ICE ITS upgrade project. (Aamodt et al., 2008).

3.1.3 The pALPIDE-2 and pALPIDE-3 sensors

The pALPIDE-2 and pALPIDE-3 chips are final-size (15 mm × 30 mm) prototypes of the ALPIDE family. The pALPIDE-2 has a pixel size 28 μm × 28 μm, while the pALPIDE-3 has a slightly modified pixel pitch of 29.24 μm × 26.88 μm (see in figure 3.6). As the pALPIDE-1, these chips also have binary output signals and the AERD. The AERD of the pALPIDE-2 is the same as one of the pALPIDE-1, while the logic of the pALPIDE-3 is built from standard cells in opposite to the full custom logic of the pALPIDE-1 and the pALPIDE-2. These prototypes are also segmented into sectors with different pixel geometries. The pALPIDE-2 has four sectors, and its characteristics can be found in Tables 3.1. The pALPIDE-3 has eight different sectors, characteristics can be found in Tables 3.2.

The main goal for the sectors in the pALPIDE-2 is to test the effect of the reset mechanism and of the spacing between the collection n-well and the surrounding p-well, but there is also a sector where the change is the size of the input transistor. This sector was expected to have a lower fake hit rate, but a higher charge threshold. The lower fake hit rate was confirmed by the measurements, but no significant change in the threshold was seen. For the pALPIDE-3, the analog front-end was further optimized to reduce the pulse length and the spread in the charge threshold values between pixels.

Other new features were also introduced in the pALPIDE-2 and the pALPIDE-3, which were missing from the pALPIDE-1. The pALPIDE-2 is the first prototype, where all the functionality to build detector modules from it are included. In the pALPIDE-3, three in-pixel memories were introduced, which derandomize the readout of a pixel. This is needed to cope with the expected

Table 3.1 Details of the four sectors of the pALPIDE-2 chip.

Sector	Spacing	Reset	Input transistor size
0	2 μm	PMOS	small
1	2 μm	PMOS	large
2	4 μm	PMOS	small
3	2 μm	Diode	small

Table 3.2 Details of the eight sectors of the pALPIDE-3 chip.

Sector	Transistor size (M_3, M_4, M_5, M_8)	Introduction of V_{CASN2}	Connection of M_6 gate	Connection of M_1 bulk	Reset	Spacing
0	optimized	Yes	diode connection	AVDD	Diode	2 μm
1	optimized	No	diode connection	AVDD	Diode	2 μm
2	as in pALPIDE-1/2	No	diode connection	AVDD	Diode	2 μm
3	optimized	Yes	V_{CLIP}	AVDD	Diode	2 μm
4	optimized	Yes	V_{CLIP}	Source	Diode	2 μm
5	optimized	Yes	V_{CLIP}	Source	Diode	3 μm
6	as in pALPIDE-1/2	No	diode connection	AVDD	PMOS	2 μm
7	optimized	Yes	V_{CLIP}	Source	PMOS	2 μm

data-taking rate of ALICE.
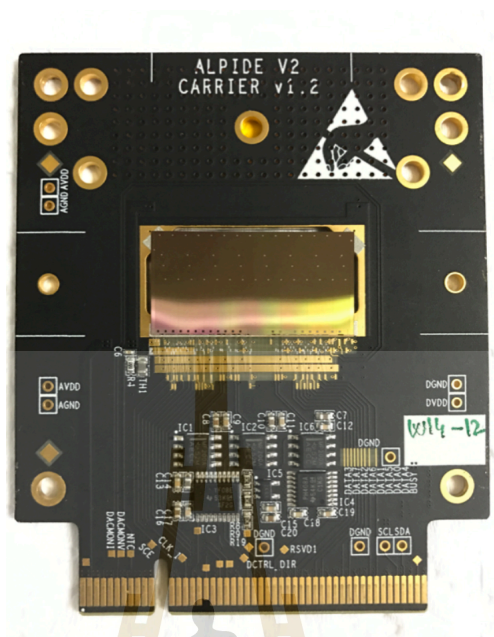
Figure 3.6 Picture of the pALPIDE-3 chip. (Aamodt et al., 2008).

3.1.4 The ALPIDE sensor

ALPIDE is the final chip developed for the ALICE ITS upgrade. It is 15×30 mm^2 as the earlier prototypes with 512×1024 pixels of $29.24\ \mu$m $\times 26.88\ \mu$m. It has only one-pixel flavor, which corresponds to sector 5 of the pALPIDE-3. It is the fully optimized analog front-end with a diode reset and a spacing of 3 μm between the collection n-well and the surrounding p-well. The large input transistor, which was found to be beneficial for the noise occupancy in the pALPIDE-2 and pALPIDE-3, was kept for the ALPIDE as well. The chip is produced with a 25 μm thick epitaxial layer, and minor modifications were introduced in the periphery to further optimize the power consumption and the tolerance to single event upsets.

3.2 Basic chip test

The functional test is a basic test for a chip. It is a test to check efficiency of a sensor, and the communication between sensors and a computer. The fuction-nal test consists of 3 tests: a First In First Out (FIFO) test, SCANDACs, and Threshold Scan.

3.2.1 laboratory test setup

A laboratory test is a functional test for a single chip sensor. To set up the experiment, there are five steps follows as shown in figure 3.7(b): (1) the firmware is uploaded by using ALTERA USB blaster to Data Acquisition Board (DAQ), (2) connecting a chip carrier board, a DAQ board, a power supply and a computer together, (3) connecting main using voltage 5.0 volts and back-bias voltage(Vbb) from a power supply to DAQ board, (4) connecting USB 3.0 ALTERA cable to PC and upload fx3 onto the DAQ board, and (5) running command to perform all test from the computer.

(a)   **(b)**
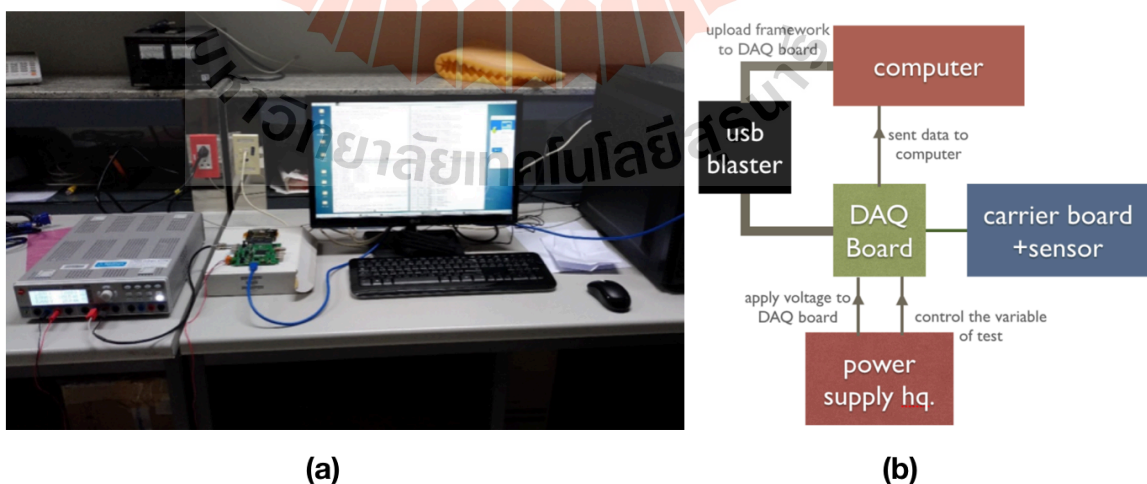
Figure 3.7 Schematics (a) the laboratory experiment and (b) drawing of the setup of experiment. (Aamodt et al., 2008).

3.2.2 FIFO test

The First In First Out test (FIFO test) is a quick test to check the Joint Test Action Group (JTAG) communication with the chip. It writes three different bit patterns (0x0000, 0xffff and 0x5555) into each cell of the end-of-column. FIFO reads them back and checks the correctness of the readback value.

3.2.3 SCANDAC

The output of the on-chip Digital to Analog Counter (DAC) (figure 3.8) can be connected to monitoring pins of the ALPIDE chip and measured by ADCs on the DAQ board. The READDAC test loops over all chip DACs, measures their output once, and prints the measured values to screen.

3.2.4 Threshold scan

The threshold scan performs analogue injections and looping over the charge. The threshold can be adjusted by varying the parameters I_{THR} and V_{CASN}. It can be observed that the threshold increases almost linearly with increasing I_{THR}. Figure 3.9 shows when increasing the reverse bias: 0V, -3V and -6V, the slope of the threshold as function of I_{THR} is reduced. Moreover, noise increases with increasing the reverse bias.
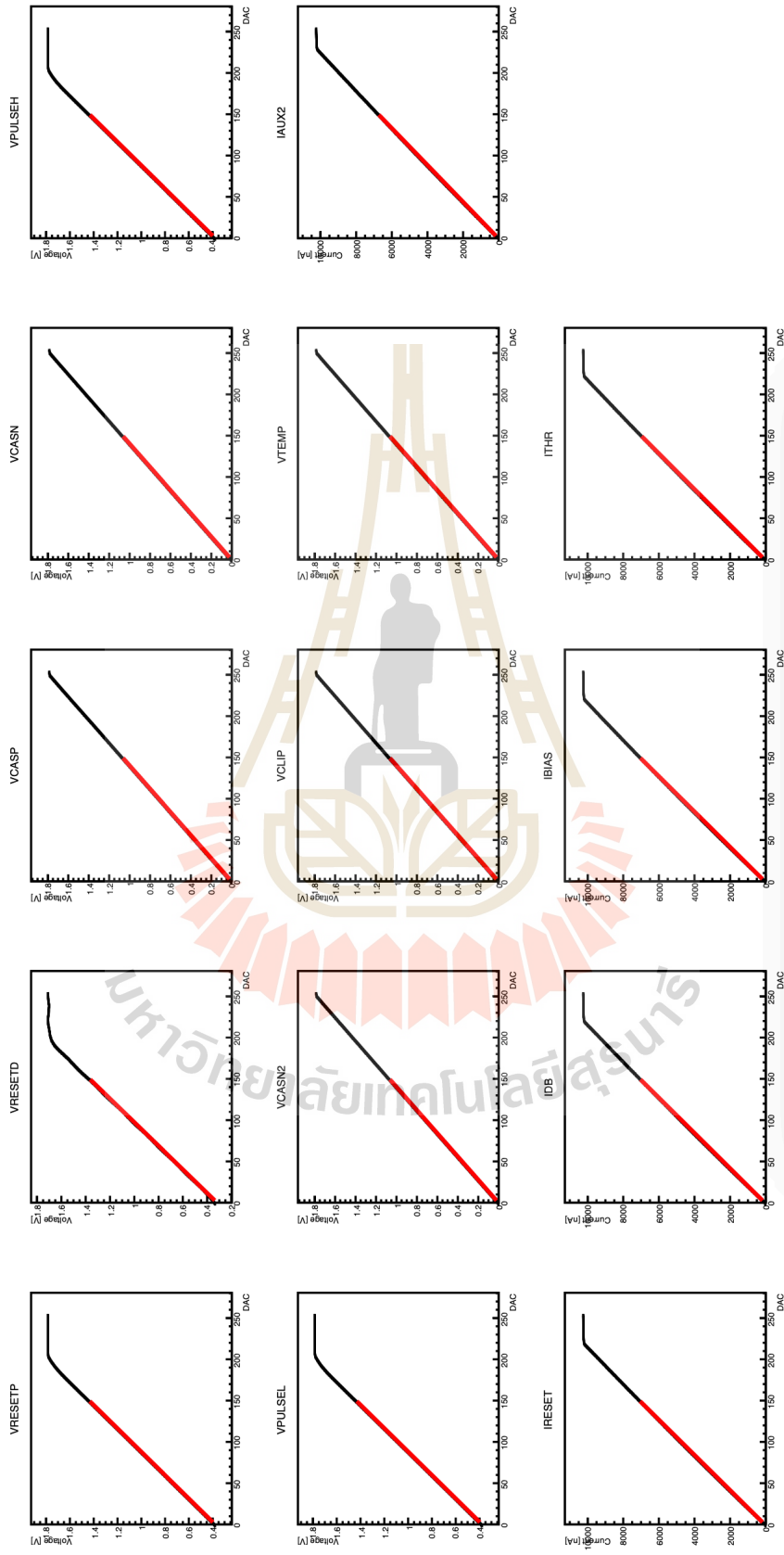
Figure 3.8 Transformation of electronic signals to the bias parameters (in DAC unit).
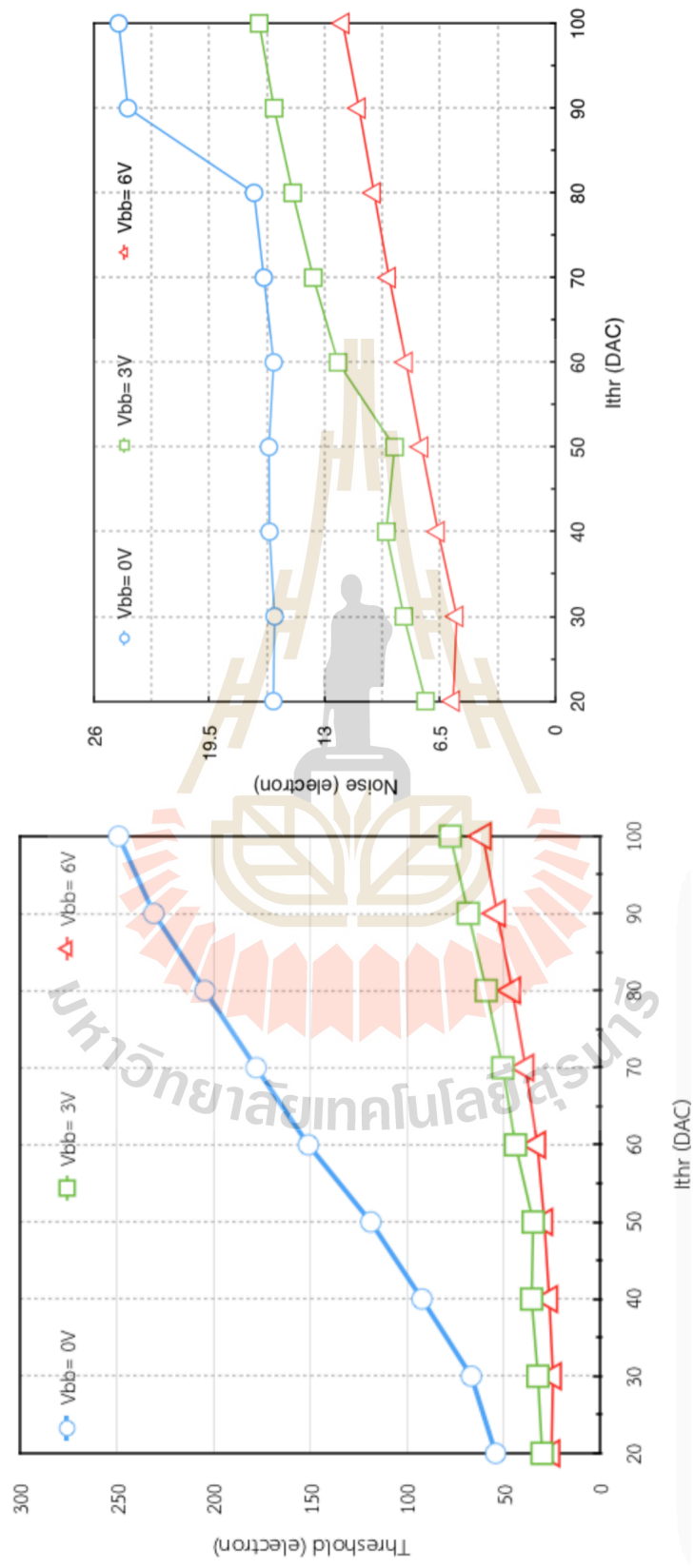
Figure 3.9 Threshold (left) and noise (right) for different V_{bb} as function of I_{THR}.

CHAPTER IV

SYNCHROTRON LIGHT RESEARCH

INSTITUTE - BEAM TEST FACILITY

4.1 Synchrotron Light Research Institute

The Synchrotron Light Research Institute (SLRI) provides synchrotron light that is produced by 1.2 GeV electron beam (Kittimanapun et al., 2017) to study fundamental science, biological, medical science and industrial research. The SLRI accelerator includes: 1. an electron gun which produces a large amount of electron, 2. a 40 MeV Linear Accelerator (linac) that provides an electron bunch, 3. a synchrotron booster that accelerates electron beams to an electron beam energy of 1.2 GeV, and 4. a storage ring where the electron beam is stored to generate synchrotron light. Figure 4.1 shows the components of the accelerator complex at SLRI.

SLRI has initiated the project that utilizes the high-energy electron beam by setting up a dedicated Beam Test Facility (BTF) (Kittimanapun et al., 2016). The aim of SLRI BTF is to produce a defined number of electrons from a few to million electrons per burst. The electron energy can range up to 1.2 GeV. The main object of SLRI BTF is characterization and testing the high energy detectors. SLRI BTF has provided sufficient beam time that serves from the current injection scheme. The facility can operate during the normal service of synchrotron light. The facility is extended from the high-energy beam transport beamline (HBT) and locates underground together with other injector components.
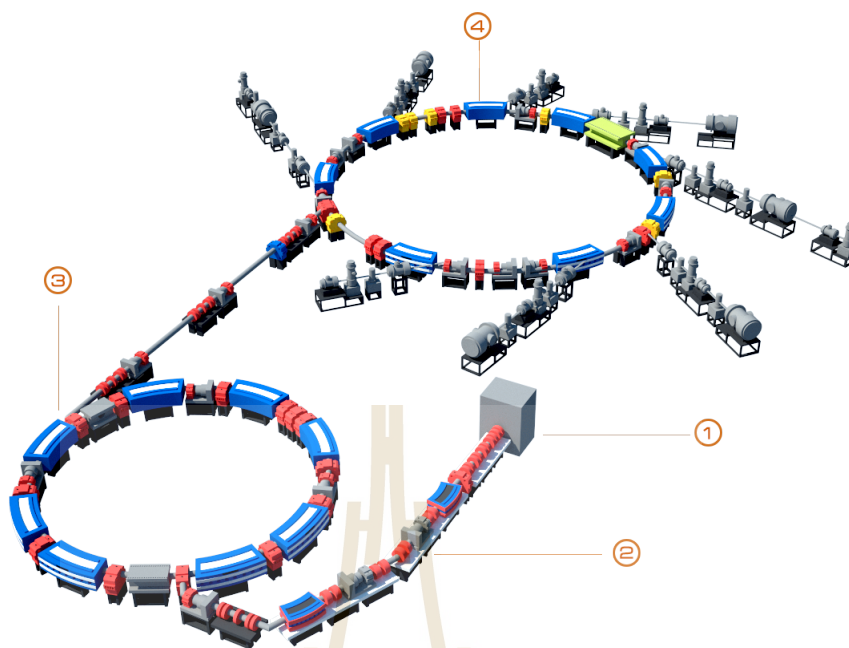
Figure 4.1 The layout of the SLRI accelerator complex (Kittimanapun et al., 2019).

4.2 Beam Test Facility

Synchrotron light research institute - beam test facility (SLRI-BTF) is an experiment station used for testing detectors properties. It is located in the basement of the SLRI accelerator building next to the vertical bending magnet (BV) where the electron beam is transported to the storage ring (SR). This bending magnet is turned off when SLRI BTF is in operation. Table 4.1 lists the electron and machine parameters at the HBT beamline.

Two target chambers have been placed at the low-energy beam transport beamline (LBT) and the High-Energy Beam Transport Line (HBT) beamline. Those targets are used to reduce electron intensity from approximately 10 mA to less than 10 electrons per burst. The tungstens placed inside the HBT target chamber with three different thickness, $1.7X_0$, $2.0X_0$, and $2.3X_0$ where X_0 is radi-

Table 4.1 Electron beam parameters at High-Energy Beam Transport Line (HBT).

Particle	electron
Energy	up to 1.2 GeV
Energy spread	-0.05%
Current	10 mA
Pulse duration	8.5 ns
Bunch length	0.5 ns
Repetition rate	0.5 Hz
# of electrons per burst	10^8

ation length, attenuates electron intensity and allows flexibility to select electron output. Traversing electrons with large transverse momentum are first absorbed at the upstream slit. While electrons with desired energy travel through the magnetic energy selector (BH), those with large energy dispersion are lost to the beam pipe inside the magnetic field region and the downstream slit. Two sets of focusing-defocusing quadrupoles (QF-QD) used to tune the beam are normally adjusted to transport the electron beam to the electron storage ring (SR). When SLRI-BTF is in operation, the vertical bending magnet (BV) that deflects electrons to the storage ring (SR) is turned off to allow electrons to transfer to the detector.

The area of the experimental station is 3.5 m×3.5 m×3 m. This area is reserved for the installation of the detector and tested instrumentation including a local computer, a power supply, and a detector system. The components of the SLRI-BTF include 1. electron gun for producing electrons, 2. a tungsten target that controls the electron intensity by varying the depth of the tungsten target
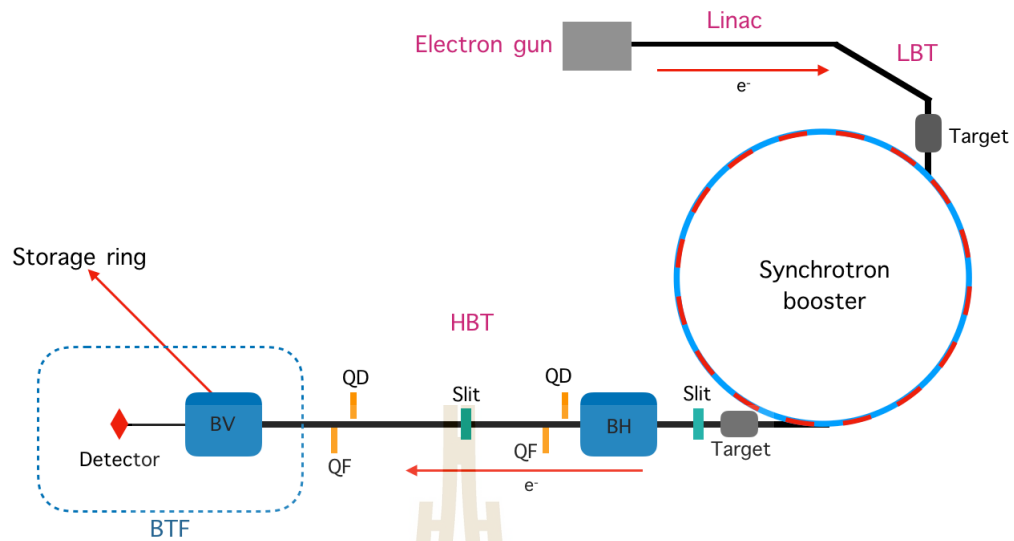
Figure 4.2 Conceptual diagram of beam test facility.

manipulator, and 3. electron beam test station (Kittimanapun et al., 2019).

4.3 Pixel sensor telescope

Almost all ALPIDE prototypes are characterized by a soft X-ray source from test beam facilities at CERN or MIPs at DESY. The primary sensor tests are performed in the laboratory, the functionality, and the collection efficiency test as described in chapter 3.2. Afterward, the ALPIDE prototypes are investigated with the particle beam. The detection efficiency and spatial resolution are measured by the beam test. The setup of measurement uses several planes of the ALPIDE sensor that are perpendicularly aligned to the particle beam. The sensor alignment is called a pixel sensor telescope. The pixel sensor telescope includes seven plane of sensors with six reference and one DUT (Device Under Test). The pixel sensor telescope is installed at SLRI-BTF for sensor characterization with a high-energy electron of 1.2 GeV.
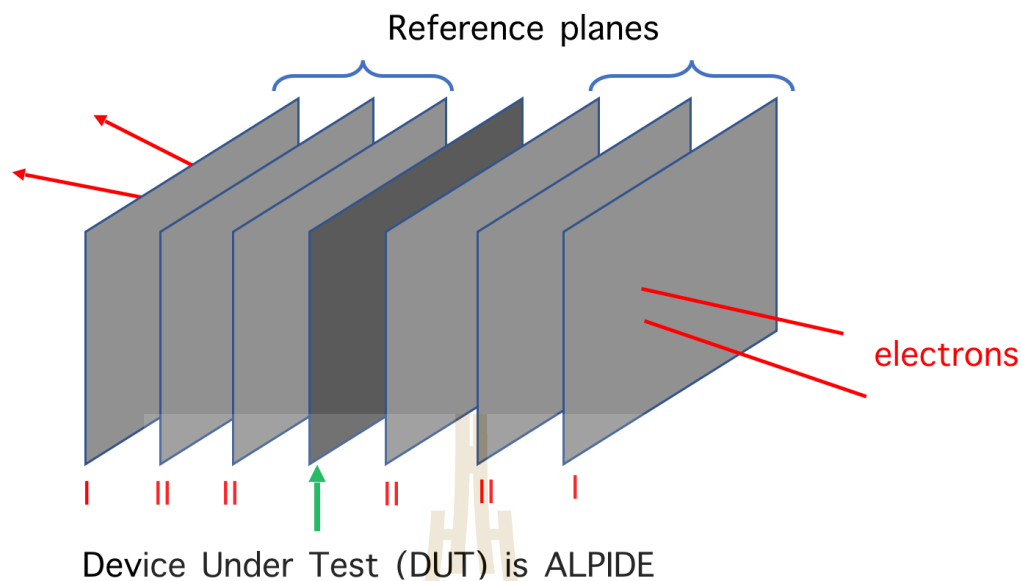
Figure 4.3 Layout the setup of first-pixel sensor telescope.

4.3.1 First-pixel sensor telescope

The first-pixel sensor telescope set up at SLRI BTF consists of seven planes of ALPIDE prototypes with 20 mm spacing as shown in figure 4.3. The ALPIDE sensor is placed as DUT in the middle of an array. The reference planes are two planes of p-ALPIDE-1 and four planes of p-ALPIDE-2. Once the particle beam passes through the pixel sensor telescope, the signal is detected and the track of the particle can be reconstructed. The analysis of data is performed by the software that is developed by ITS upgrade team based on the EUTelescope framework (Perrey, 2014).

The telescope was set up and installed at SLRI-BTF for characterization of the ALPIDE sensors. The information of chip and back bias voltage for each plane of the first-pixel sensor telescope is shown in the Table 4.2. The goal of the characterization is to measure the detection efficiency of the ALPIDE sensor. The EUDAQ software is used to collect the raw data from the experiment. After that the analysis of the raw data has been performed using the EUTelescope framework

Table 4.2 The setup of first-pixel sensor telescope at SLRI BTF.

Plane number	Chip ID	Chip type	Back bias voltage
1	W9-17	pALPIDE-1	0
2	W14-18	pALPIDE-2	-3
3	W14-9	pALPIDE-2	-3
4	A4-W7	ALPIDE	-3
5	W14-12	pALPIDE-2	-3
6	W14-25	pALPIDE-2	-3
7	W8-30	pALPIDE-1	0

(DESY collaboration, 2013).

4.3.2 Characterization of the first-pixel sensor telescope

The first-pixel sensor telescope is installed for the sensor characterization at the SLRI-BTF with a 1.0 GeV electron beam. The significant parameters to be observed are raw hit map, correlation, the number of clusters, cluster size, hit vs plane and hit vs event. These parameters verify that the telescope can detect the electron beam from SLRI BTF by the EUDAQ software. Afterwards, the raw data from the experiment were taken from the EUDAQ software and analyzed by the EUTelescope software for measuring detection efficiency of sensors in the pixel sensor telescope.

The results of the first pixel sensor telescope with a 1.0 GeV electron beam at SLRI BTF are as follows:

Raw hit map

The raw hit map graph shows the hitting position of the particle on sensors
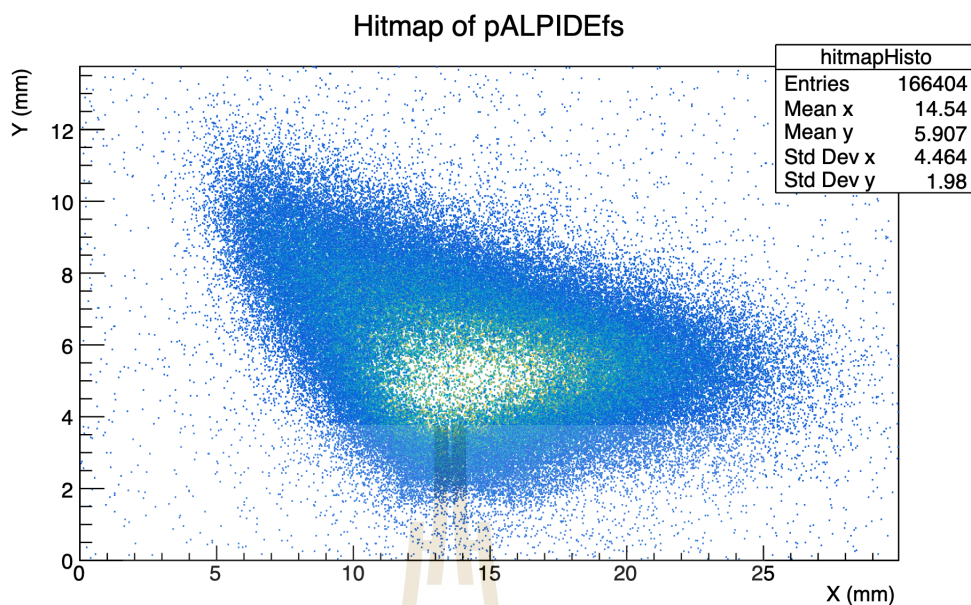
Figure 4.4 The Raw hit map of seven planes of sensor from the first-pixel sensor telescope.

for each plane from the pixel sensor telescope. The raw hit map can be observed by using EUDAQ software. The result of the raw his map is used to verify that all sensors in the pixel sensor telescope can detect incoming electrons. The distribution in figure 4.4 shows the position of electron passing through the pixel sensor telescope. The x-axis and the y-axis are the number of pixels in the horizontal and vertical of the sensor respectively. The raw hit map shows that the region the electrons passing through the most is around the center of the sensor.

Correlation

The correlation plot shows the correlation of the position in x- and y-axes that particles traverse two different planes of the pixel sensor telescope. During the test ongoing, the diagonal line should appear in the correlation plot as seen in figure 4.5. The meaning of the line is particles that traverse at the same positions on nearby chips. It confirms that the electron beam passes through the pixel sensor telescope in a straight line.
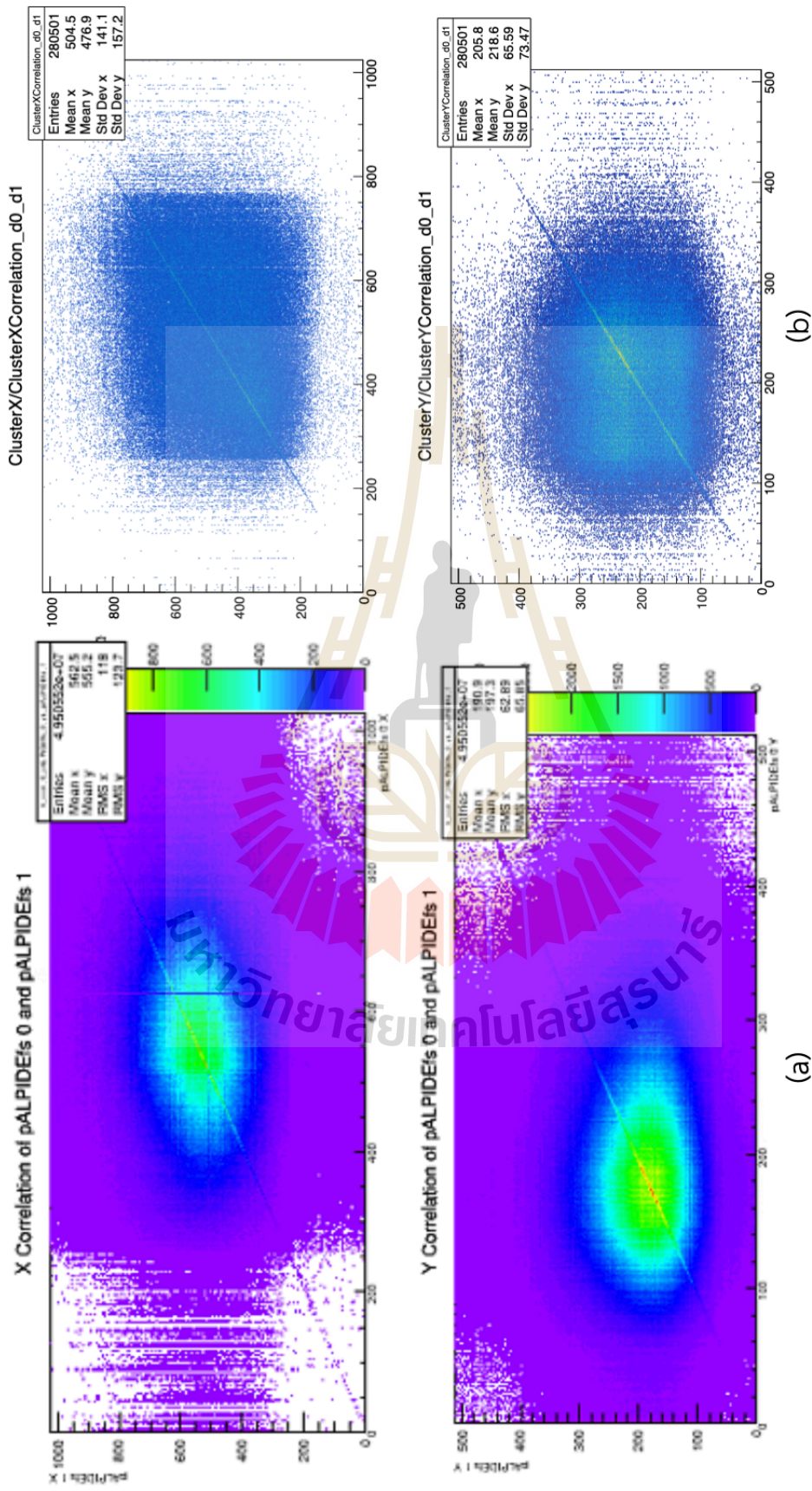
Figure 4.5 Correlations plot of the first plane with the second plane in the x and y positions, (a) raw data, and (b) after reconstruction.

Moreover, figure 4.5 shows the correlation plot between the first plane and the second plane in the x- and y-position. The x-axis is a track position of the first plane and the y-axis is a track position of the second plane. The left figure shows the graph that is plotted by using the raw data and the right figure shows the graph that is plotted by using the reconstruction data. After raw data reconstructed, we can see the relation of track position as a straight line. The distribution disperses around the linear line. It is an effect of the background, the low energy electrons that spread around the laboratory room. However, we cannot clearly distinguish between correlation and background.

Cluster size

When a charged particle passes through the pixel sensor telescope, it generates charges inside the sensor. Some charges may diffuse to other pixels near the hit pixel. Afterward, the electronics signal will be created. The total signal will be shared by several pixels. The group of pixels that create electronics signal after a particle passing through, is called a cluster size. Figure 4.6 shows distribution of cluster sizes of test beam by the pixel sensor telescope. Normally, the cluster size distribution depends on the settings of different parameters of the chip such as the operating environment and the momentum of the measured particles. In a case that signal generated by only one pixel, not a cluster, it corresponds to the noise signal coming from bias voltage given to the sensors at threshold current equal to 50 DAC unit in our test.

Number of cluster

A bunch of electrons is generated at SLRI BTF by using the target manipulator. The number of electron per bunch can be fewer than 10 electrons to million. When a bunch of electrons passes through the pixel sensor telescope, the number of clusters have been generated in a pixel sensor. Figure 4.7, the horizontal axis is
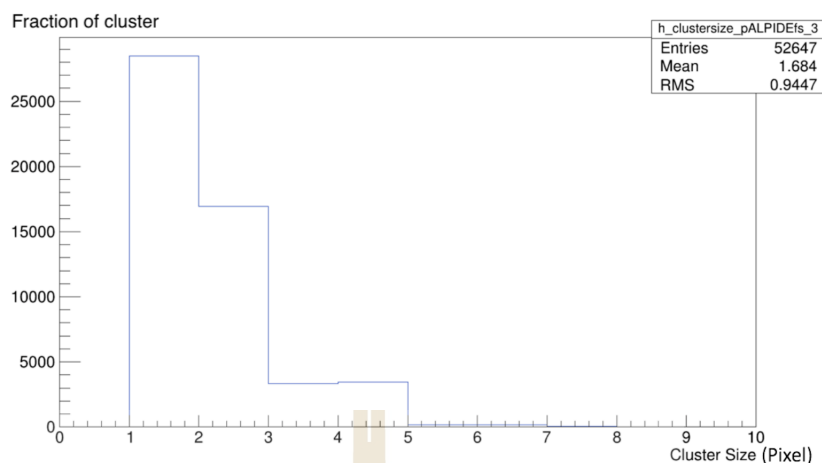
Figure 4.6 Cluster size of DUT, horizontal axis is the cluster size and vertical axis is the number of entries in each cluster size.

the number of clusters, and the vertical axis is the number of event. The number of clusters can be found as a mean value. The meaning of the number of clusters is a number of particles that hit on one pixel sensor. The average of hit number of electrons is 31.32 electrons.

Hit vs plane

Hits vs plane plot shows the number of particles that hit on each plane of the pixel sensor telescope. Figure 4.8, the horizontal axis the number of sensor plane and the vertical axis is the number of particles that hit on each plane. The pALPIDE-1 sensors are placed at the first and the last plane. The graph shows the average number of hits that the first and last planes can detect is between 40.2 to 42.8 hits. The pALPIDE-2 sensors, the second, third and fifth planes can detect the average number of hits around 47 hits. Only the sixth plane can detect the average number of hits between 58.0 to 58.8 hits. The ALPIDE sensor is placed at the middle plane as the DUT can detect the average number of hits between 58.8 to 60.0 hits.

The ALPIDE sensor can detect the average number of hits better than
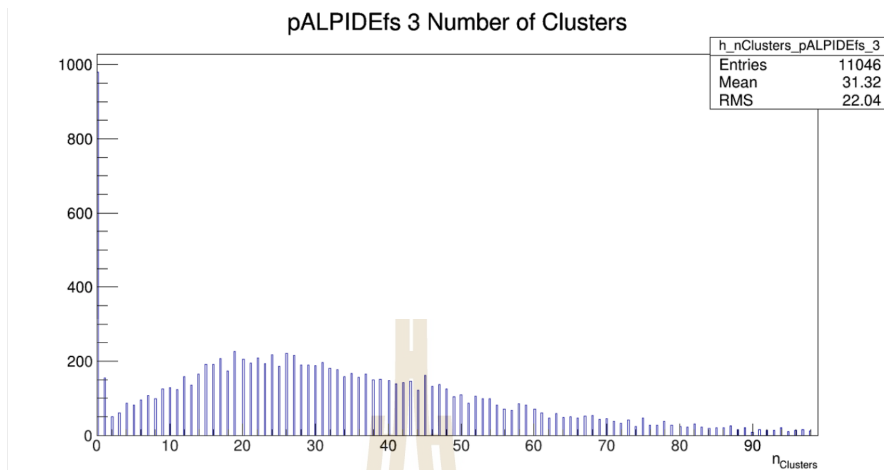
Figure 4.7 Number of clusters of DUT, x axis is the number of cluster and y axis is the number of entries in each number of cluster.
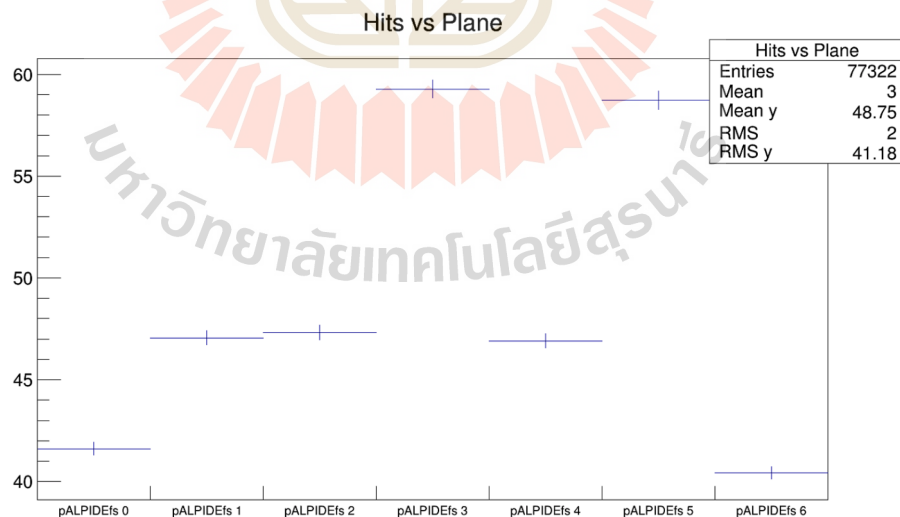
Figure 4.8 Number of hit for each planes of pixel sensor telescope. The x-axis is the number of plane and the y-axis is the number of particles that hit on sensor.
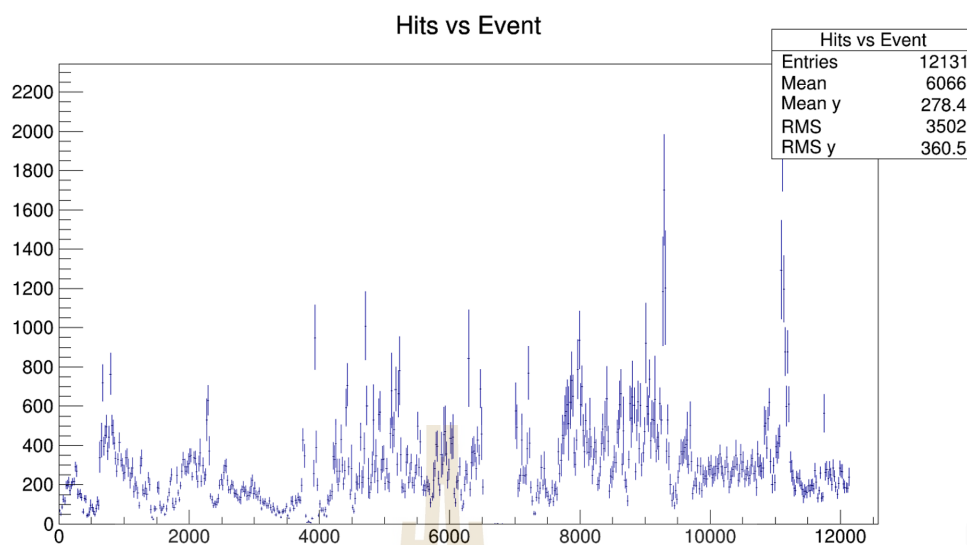
Figure 4.9 Hit per events of the ALPIDE sensor, x-axis is the number of event, and y-axis is the number of particles each number of events.

pALPIDE-1 and pALPIDE-2 as expected. However, there is one pALPIDE-2 in the sixth plane that detect the average number of hits better than other pALPIDE-2. It may be affected by the different quality of wafers used in the production of the pALPIDE-2 or different production lots at silicon chip foundry.

Hit vs events

Figure 4.9, hits vs event plot shows the total number of particles that hit on the pixel sensor telescope for each event. The horizontal axis is the number of events, and the vertical axis is the total number of particles hits the pixel sensor telescope. The events are the number of particles that collide the sensor.

After the data is collected. The raw data has been analyzed by using the EU-Telescope framework. The important parameters, detection efficiency, and spatial resolution are calculated.

Detection efficiency

After the ALPIDE sensors with the new version of pixel sensor telescope were measured by using the 1.0 GeV electron beam at SLRI. In the analysis part, the detection efficiency, and spatial resolution are calculated. All tracks can be used to calculate the detection efficiency. The detection efficiency is given by a ratio of associated hit to all particle tracks and all particle tracks from a telescope as the equation,

$$\text{Detection efficiency} = \frac{\text{An associated tracks with hit on DUT}}{\text{All tracks on DUT}}$$

The ITS upgrade project requires the detection efficiency for tracking particle to be higher than 99%. The calculation of detection efficiency considers the ratio of tracks hit on DUT and all tracks on DUT.
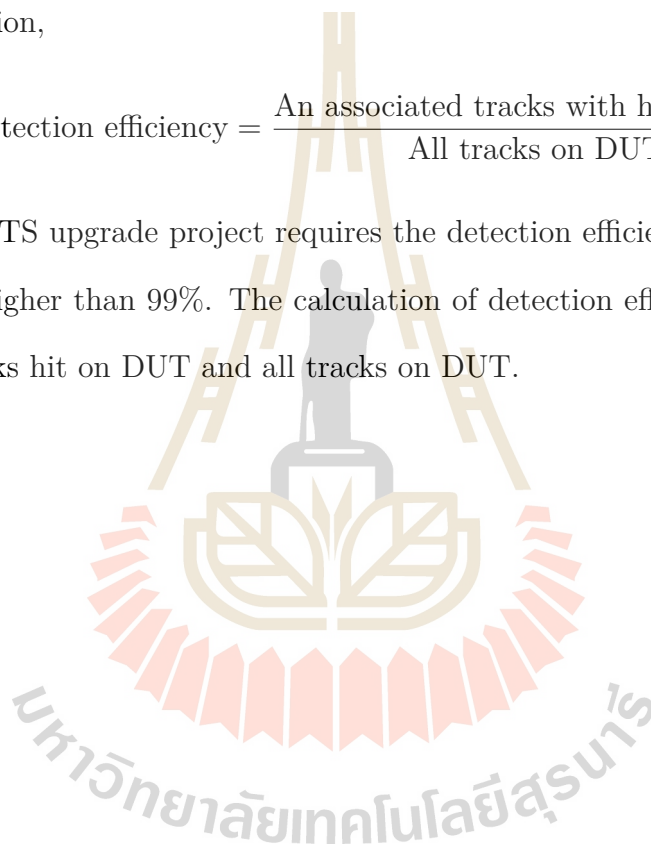
CHAPTER V

UPGRADE OF PIXEL SENSOR TELESCOPE

There are three main topics in this chapter. First, we explain the software that is used to simulate the particle trajectory. This software was designed to use for the ALICE ITS upgrade, when the sensor chip was tested with variant beam energy (vary the setup value of facility). Next topic shows the process of the modification of the new pixel sensor telescope, including the parameter adjustment. The last topic is our contribution to the ALICE surface commissioning process. This section also shows the progress of the ALICE ITS upgrade project from the late of 2019 to the middle of 2020.

5.1 Trajectory prediction

To predict of reconstruct particle trajectories recorded within a new pixel sensor telescope, requires a comprehensive software framework. First, the Monte Carlo method is introduced. This method is computational algorithms that rely on repeated random sampling to obtain numerical results. Moreover, this method is also used in a simulation for the ALICE ITS upgrade project, which is called the telescope optimizer.

5.1.1 The telescope optimizer

Prior to the construction of the new pixel telescope, a telescope optimizer was used to predict the trajectory of particles to the pixel sensor telescope. Additionally, the telescope optimizer makes it easy to specify a suitable boundary

for the experiment. The telescope optimizer calculates the track position using the Monte Carlo (MC) method. The track position establishes the trajectory of particles that move though the pixel sensor telescope (Mager, 2016). The track position determines whether a charged particle has traversed the material with small random deflections due to the multiple scattering (Scandale et al., 2017). Multiple scattering affects the energy loss of a particle in a matter and the deflected direction of an incident particle. The interaction mechanism depends on the momentum, energy, and charge of an incident particle.

The calculation boundary is the input obtained from the telescopic parameters. The spacing between the reference planes, in our case, is 20 mm, and the spacing of between the DUT and the reference planes is 40 mm. The spatial resolution of all planes is 5 μm and the material budget (x/X0) per layer is 0.5 %. Figure 5.1 shows the general track position and figure 5.2 shows the track position calculated using the MC method. The green line indicates the particle trajectory obtained using the values from the MC method. The black lines indicates the possible trajectories of particles moving through the pixel sensor telescope.
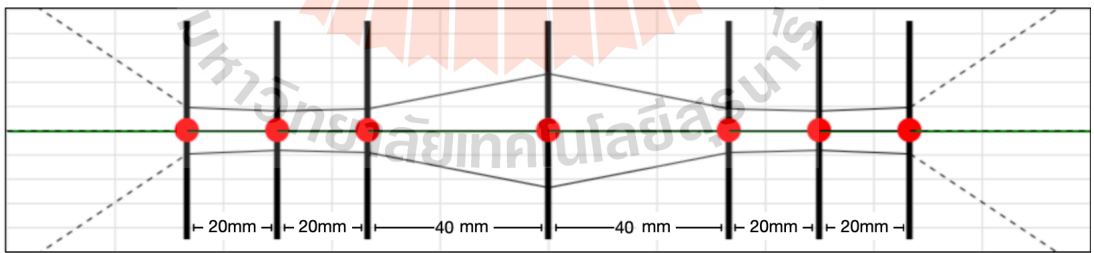

Figure 5.1 General track position.

5.2 Modification of telescope setup

This work focuses on the characterization of ALPIDE sensors with the new version of the pixel sensor telescope using the 1.2 GeV electron beam at SLRI. A
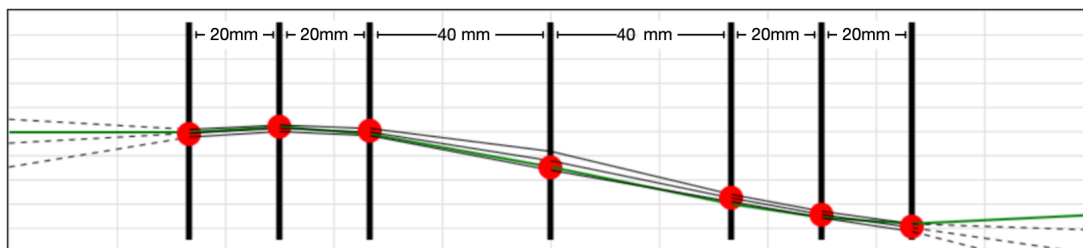
Figure 5.2 Monte Carlo track position.

diagram of the new sensor telescope is shown in figure 4.3 The new sensor telescope consists of seven planes of the ALPIDE sensors. The chip is placed in the middle plane (the DUT) while the other planes are the reference planes. The telescope is upgraded so that it can move the DUT plane along the transverse plane (x- and y-directions). It has a resolution of 0.1 mm, and a 10 mm stage (range in the vertical and horizontal directions). The new pixel sensor telescope is currently being constructed at the SLRI-BTF.

The telescope cannot be used to characterize other areas. However, the competence of the new telescope enables other sections of the sensor in the DUT to be measured such as its edges and corners. This advantage provides us with a complete view of the detection efficiency in all sections of the ALPIDE sensor. Thus, the new pixel sensor telescope can determine the complete quality of the ALPIDE sensor.

5.3 ALICE surface commissioning

In this section, we present our contribution starting from July 2019 - Dec 2019 to the ITS surface commissioning 2019 at CERN for 6 months. For this process, ALICE requested manpower from each institution which is a full member of ALICE and participates in the ITS upgrade project to help with the surface commissioning. This operation began after the full detector layers were assembled in

a clean-room at CERN, the cooling system and the collecting data were connected to each detector layer.

5.3.1   Installation of the detector layer at CERN

The commissioning hall has been placed at building 167, CERN. It is divided into three rooms with different functionality as follows.

Clean room

The clean-room is built to use for assembling the detector layer. This room is used for assembling the detector layers of the ITS. The detector layer is installed to test the electronic signal quality. The assembly requires high precision and cleanliness for a sensor. Therefore, it is necessary to assemble and install the detector in a clean-room to quarantine dust that could adversely affect the detector.
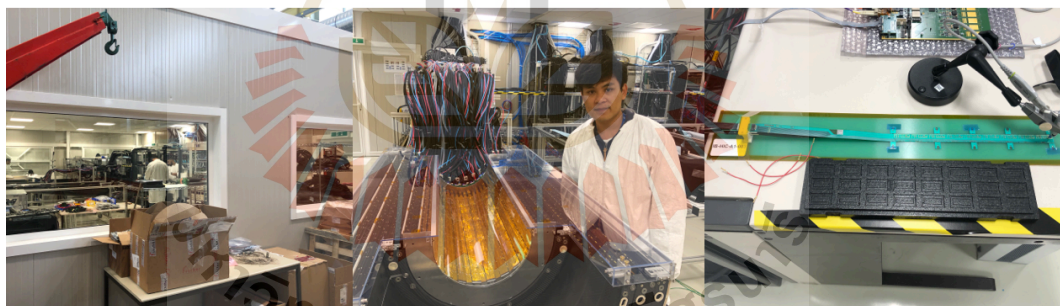
Figure 5.3 The commissioning hall. The assembly operation can be seen from outside (left). Real-size of the detector layer compared to the researchers (middle). The stave to be installed as a detector layer (right).

Control room

A personal computer is used to control and monitor the detector layer in the cleanroom. The characterization is controlled by a researcher (shifter) to test a detector layer in each day/time, to collect data of a test. Moreover, the control room is also used as a daily meeting place to summarize and discuss about the progress of the ALICE ITS upgrade.
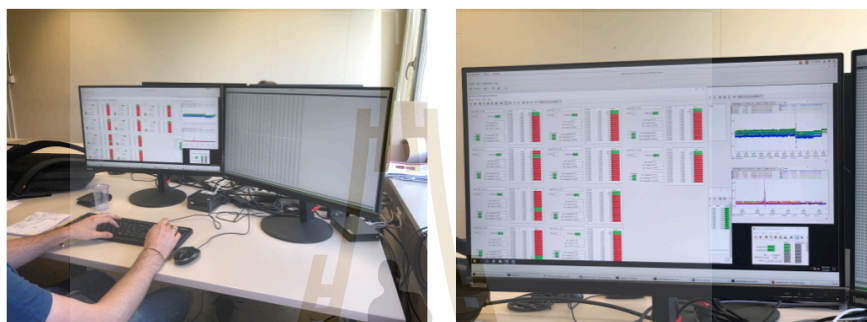
Figure 5.4 The picture shows the operation while controlling the detector layers.

Cooling room

The cooling system is installed in this room. This system includes the cooler, cooling cables and pipes, and the cooling control panel. The storage system or the water tank is also installed in this room.
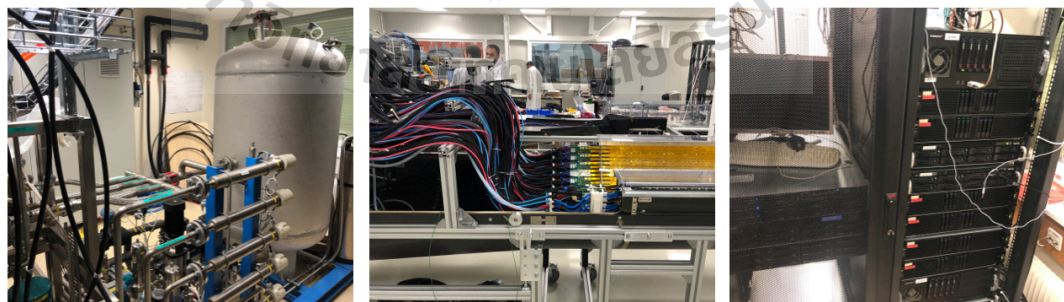
Figure 5.5 Components of the cooling room. The cooler (left). The cooling pipes that connect from the chiller to the detector layers in the cleanroom (middle). The data collection system (right).

5.3.2 Performance testing of the detector

The detector layer is divided into 2 components. The first component is the Inner Barrel (IB) which consists of by Inner Barrel Top (IBT) and Inner Barrel Bottom (IBB). The Outer Barrel Top (OB-T) and Outer Barrel Bottom (OB-B) were assembled as the Outer Barrel (OB) of the second components. The characterization of a detector layer is performed layer by layer. After that total the preliminary detector's performance will be obtained. The goal of this test is to check the basic performance of the new ITS detector before moving to install as a central part of the ALICE detector at the ALICE cavern (point 2) of the LHC ring. The details of testing are determined by experts. Each week, there is a definite plan and purpose for which detector layer to be tested, and which parameters to be observed. This section shows the routine, test methods, and data collection methods of quality performance. In the surface commissioning process, the main quality test is contained with three steps those are 1. electronic quantities test, 2. QC calculation for an error in sensor and 3. monitoring a physics parameters.

Electronic quantities test: this test is done every one hour

- Threshold Scan: The objective of this test is to check the threshold of every pixel in the chip (or the full detector layer) that should have the same values, or should be consistent. This value is the measurement of the charge collection that occurs during a particle hits over that pixel. The result of the threshold scan is shown in figure 5.6.

- Fake Hit Rate: This is defined by the number of particle collisions per pixel in each event without the external disturbance. This test measures the noise of the detector. During commissioning, there is no real particles passing through sensor.

- Readout Test: This is an electronic signal transmission test that observes the signal transmission between the detector layer and a computer. This test will be stopped when the next routine test is started. The detector's status is indicated by using the readout test. If the test is stopped with any notification, it means that there is some communication problems between the detector layer and the computer.
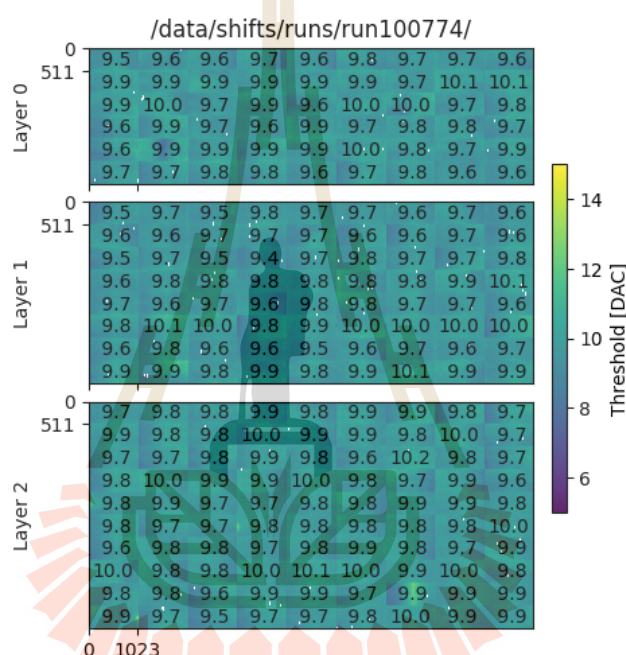
Figure 5.6 This figure shows the threshold of the inner barrel top, including detector layer-0, detector layer-1, and detector layer-2 in all pixels.

QC calculation for an error in sensor

QC is tested after the FakeHitRate test is completed. QC takes the data from the FakeHitRate test to calculate where the error occurred on the detector layer. The test ID will be divided into 11 parts as shown in figure 5.7. This figure shows the Occupancy versus Chip and Stave for each layer of the Inner barrel. It tells us about the number of particles in each chip. Moreover, the occupancy distribution indicates the distribution of particles through each sensor.
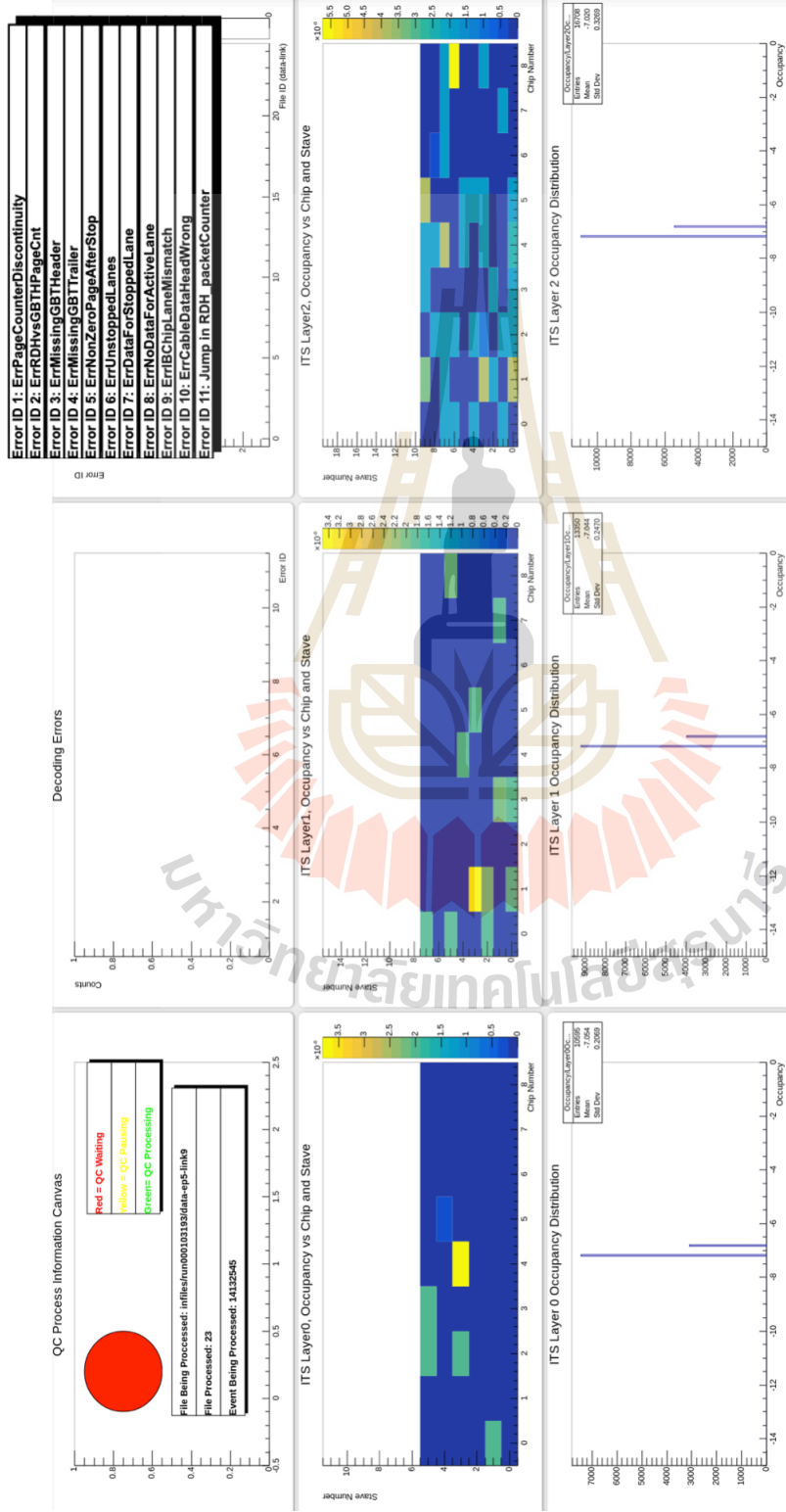
Figure 5.7 QC calculation monitor. The first row shows an error of the 11 error ID. This result tells us that tests out of error. The second-row shows an occupancy vs chip/stave and the third-row shows an occupancy distribution of detector layer-0, detector layer-1, and detector layer-2 respectively. (Aamodt et al., 2008).

Monitoring a physics parameters

This step is to see what happens inside a sensor. The important variable is the temperature of the detector layer which is an important factor in the actual measurement. The electricity and the electric potential are also monitored. The physics variable must be checked every 10 minutes of all detector layers.
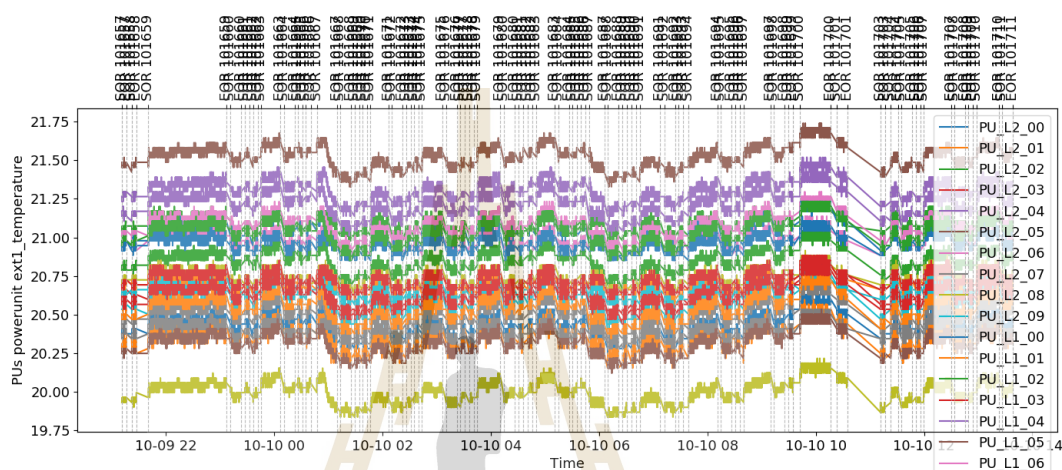

Figure 5.8 Inner barrel-top (IBT) temperature stability during the 50 runs. The stave is classified by a different color.

5.3.3 The summary of the surface commissioning at CERN

The performance tests of the inner tracking system (on the surface commissioning) are ThresholdScan, FakeHitRate (continue with the QC test), and ReadoutTest. These tests have collected a lot of data and sent them to the server. The ALICE team transfers the data every 2-3 months, and take all the data sets for a complete analysis.

The surface commissioning is going as planned. The inner barrel has been tested 80% of total integrity, another 20% is testing the outer barrel. Moreover, all seven layers of the detector have been assembled to test with the electronics and cooling systems. The surface commissioning is expected to complete in July

Table 5.1 The table show as a part of the experimental results of the characterization, the surface commissioning of the inner tracking system.

	THRESHOLD	FAKE HIT RATE	READOUT	QC
TOTAL	82	68	63	48
Good	67	68	61	48
Warnings in readout.exe	3	0	0	0
Check RU counters	3	0	0	0
Check CRU counters	5	0	2	0
Exceeded retries	2	0	0	0
Command timed out	1	0	0	0
DCS didn't send sequence	3	0	0	0
Not clear or missing info	4	0	0	0
TOTAL ERROR	15	0	2	0
FRACTION OF PROBLEMATIC RUNS	22.38%	0%	3.28%	0%

2020. After that, the inner tracking system will be disassembled and moved to the ALICE cavern (point 2). In the underground commissioning, the installation will be performed throughout the year 2020 until the early of the year 2021. The process of installation and test are similar to the surface commissioning. The ALICE detector will be put into full operation in the second half of the year 2021 which is a six-month delay due to covid-19 situation.
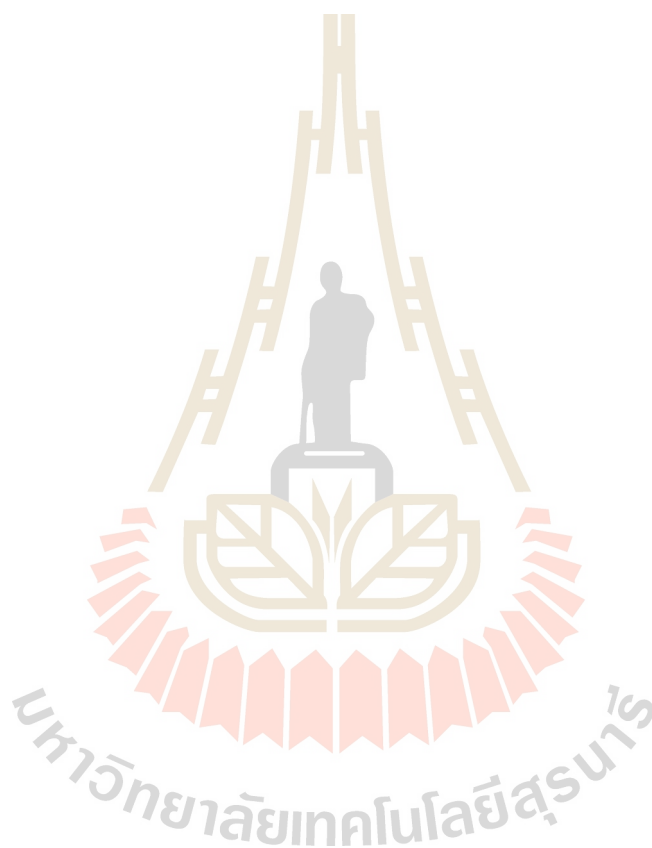
CHAPTER VI

SIMULATION RESULTS AND DISCUSSIONS

The simulation of the pixel sensor telescope is important to provide the prediction of the experiment. The G4beamline simulation used for this work, is based on the GEANT4. G4beamline is a particle simulation that is used to optimize and design beamlines. It can realistically simulation particle trajectories in the electromagnetic field and matter.

6.1 G4Beamline simulation

G4beamline is a particle tracking simulation software (Roberts et al., 2008). The software is based on GEANT4 (Agostinelli et al., 2003), a toolkit for the simulation of the passage of particles through matter. It is optimized for simulating beamlines and is especially beneficial for muon, proton and electron facilities. It can also simulate systems not organized as a beamline. Moreover, it is well suited for explaining questions about particle interactions and tracking. The tracking of particles through the G4beamline is as accurate and realistic as the GEANT4 toolkit. G4beamline is an open-source program distributed for Linux, Mac OS X, and Windows.

The concept of this work are as follow, the Device Under Test (DUT) is rotated around a y-axis. The simulation starts with the changes of the DUT angle from 0, 10, 20, 30 and 40 degrees. Reference planes are at fixed angles of 0 degree. In the part of the electron beam properties, this simulation uses the beam data from the SLRI-BTF beam test results. The beam data was obtained from the

ROOT file that was result from the pixel sensor telescope characterization (current telescope). However, the background noise are not added to the simulation. This work cannot put the background because the exact background values cannot be found. So, the electron beam is accelerated to 1.2 GeV, with gaussian distribution of 0.5-cm FWHM in a transverse plane, and 60-MeV FWHM in energy. The number of events is 166,404 and used as a single particle. In the part of the ALPIDE sensor, the seven detectors are created on the simulation as a silicon detector with the atomic number of 14, the atomic mass of 28.0855 g.mol^{-1}, and the density of 2.57 g.cm^{-3}. The setting parameters of the upgrade pixel sensor telescope is taken from section 5.1.1.
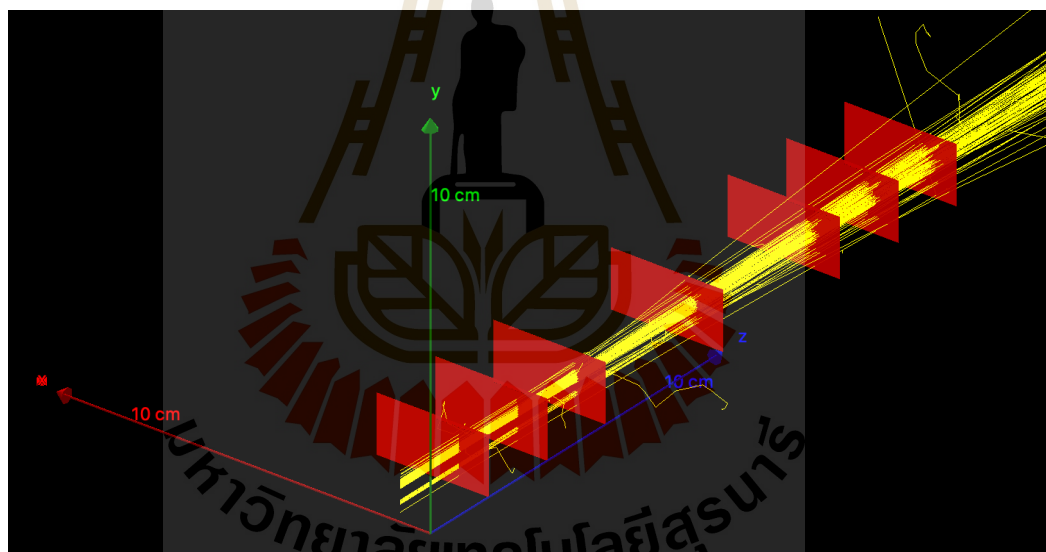
Figure 6.1 The layout of G4beamline software is shown. The electron beam passes through seven silicon sensors used as a pixel sensor telescope with the angle of the DUT plane to be 0 degrees.

This work started with an angle of the DUT plane of 0 degree. The electron beam has been moving to those sensors along the z-axis (see in figure 6.1). The raw root file is created when the simulation finishes. The next simulation will starts after the angle parameter of the DUT plane is changed to 10, 20, 30, and

40 degrees around the y-axis as shown in figure 6.2. This work is divided into five scenarios, to predict the characteristic of ALPIDE when an angle of DUT is changed from 0, 10, 20, 30,40 degrees. The next section gives the results of the simulation by using the ROOT to analyze each scenario.
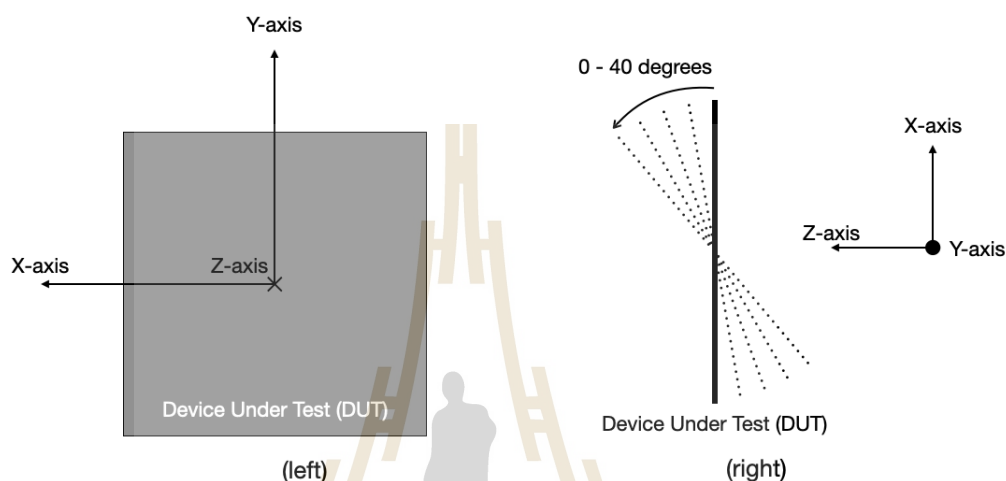
Figure 6.2 Front view (left) and top view (right) of DUT in G4beamline software. The angle of the DUT plane is chagned from 0 to 40 degrees counterclockwise around the y-axis.

6.2 Analysis of G4beamline result

A ROOT file is created after the G4beamline simulation finished. The CERN root (Brun and Rademakers, 1997), which is a framework for data processing, can help us to get the details of the simulation for processing data. ROOT is designed for particle physics data analysis, written in C++. This work focus on the study of the pixel sensor telescope in case that the angle of the DUT plane is changed.

6.2.1 Beam profile of pixel sensor telescope

The beam profile of this simulation is an electron hitmap on each sensor, a track position that electrons pass through the ALPIDE sensor. Figure 6.3 shows the beam profile of the upgrade of the pixel sensor telescope. The seven canvases represent the seven ALPIDE sensor. The x-axis of the canvas is 15 mm which is a width of the ALPIDE sensor. The y-axis of the canvas is 30 mm which is a length of the ALPIDE sensor. The explanation of this figure is the position of all-electron those are tracked by each ALPIDE sensor. The beam profile of the first plane spreads around the center. The shape of the beam profile is similar triangle cluster. When the electron is moving to the next sensor, the shape of the cluster is dispersed. The number of entries slightly decrease after the electrons moves to the next sensor.
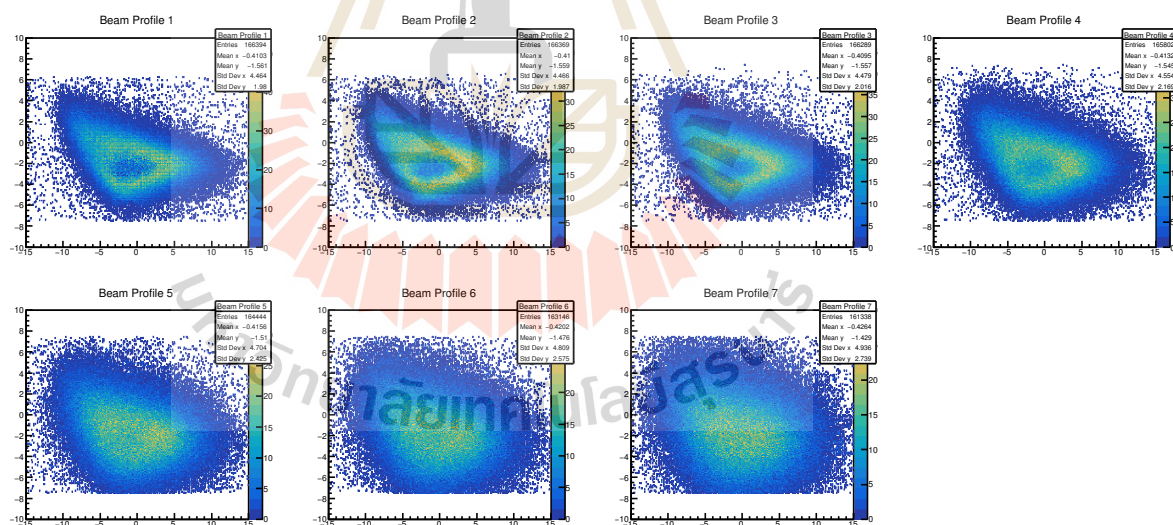

Figure 6.3 Beam profile of a pixel sensor telescope in the case angle of the DUT is 0 degrees. The beam profile is performed by using G4beamline software to do a simulation and using ROOT to analyze.

The impact of changes DUT angle is considered. Figure 6.4 shows the beam profiles of the DUT plane with a varying angle from 0, 10, 20, 30, and 40

respectively. The cluster of the beam profile is more dispersed along the y-axis of the canvas when the angle is changed to higher values.
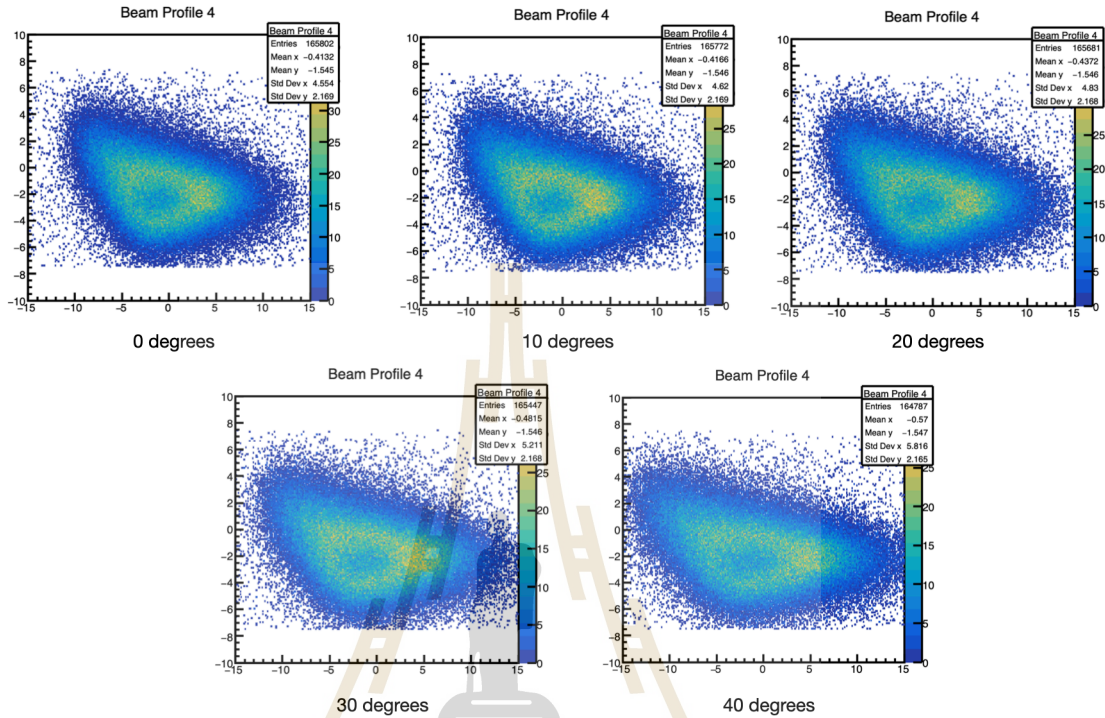
Figure 6.4 Beam profile of the DUT plane when the angles are 0, 10, 20, 30, and 40 degrees

6.2.2 The correlation

The correlation is the position of the particle passing the x-axis and y-axis between two different planes. Figure 6.5 shows the correlation-x of the DUT plane with the other 6 planes. The appearance of this correlation is similar to a linear line. Theoretically, when a single particle passes through two sensors/detectors, the track position of the first sensor/detector should be the same or close to the track position of the second sensor/detector. So, the distribution of the correlation graph can be described by this concept.

The correlation-x of DUT with the 1st plane is more dispersed than the

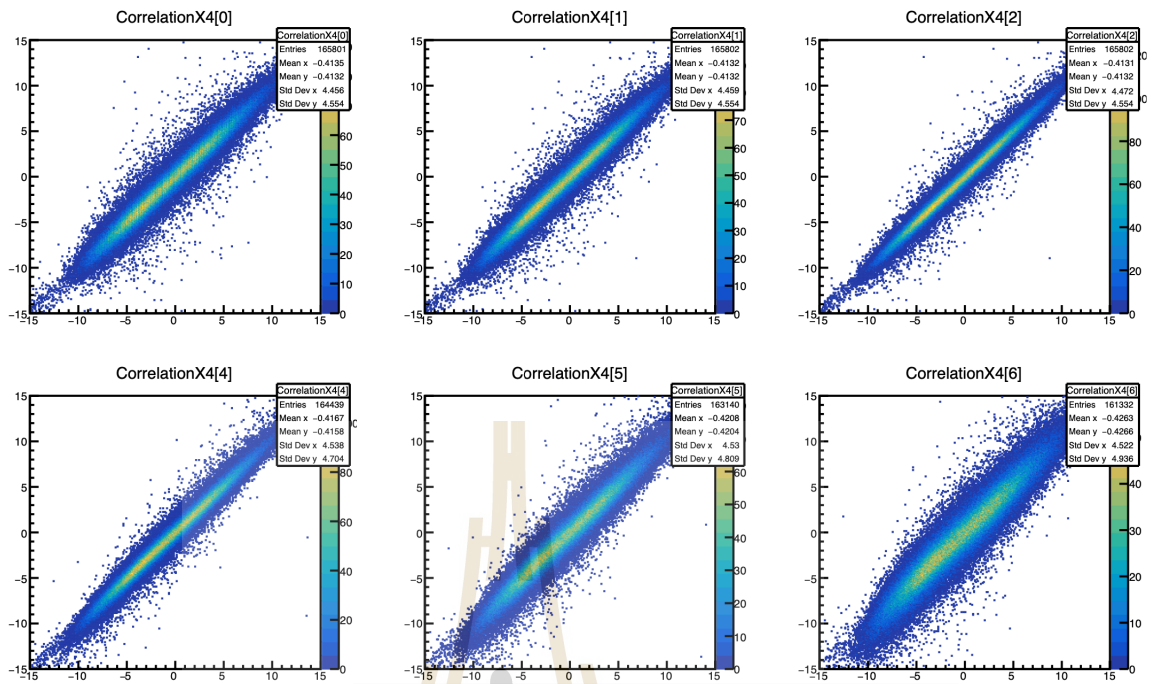**Figure 6.5** Correlation plot where the x-position of the DUT plane are plot with the x-position of the other 6 planes.

correlation-x of DUT with the 3rd plane. This can be explained by the number of sensors/detectors that the electron passing through. The multiple scattering would be suitable to answer this question (see section 2.3.5). The angle of scattering increases when an electron traverses more number of sensor/detector.

6.2.3 Prediction of scattering angular

This work aims to predict the scattering angle of the new pixel sensor telescope by using the simulation from G4beamline. The scattering angle concept can be explained in the schematic, the simulation in figure 6.7 (left) shows a track on the ALPIDE sensor plane i and a track of the same electron on the ALPIDE sensor plane $i+1$, the difference of position is Δx and Δy. The difference of all-electron track can be obtained from the correlation, which can be called delta. Moreover, the delta position of all track is shown in figure 6.8, which is
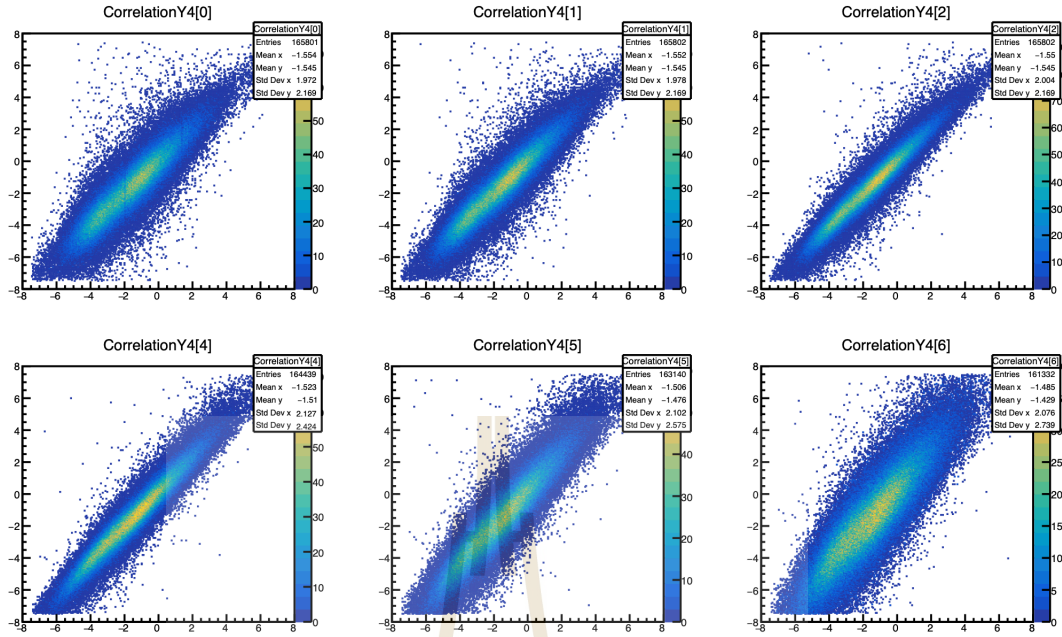
Figure 6.6 Correlation plot where the y-position of the DUT plane are plot with the y-position of the other 6 planes.

the distribution of the close plane (plane *i* and *i+1*). This "Deltahis" graph is the difference between the track position of the DUT plane with the other planes. For example, a single electron with a particle ID = 10 is passing through the first sensor/detector at $x = 10$ mm and $y = 15$ mm, then it passes through the second sensor/detector at $x = 12$ mm and $y = 20$ mm. So, the total Deltahis of an electron ID = 10 is $\Delta x = 2$ mm and $\Delta y = 5$ mm.

The Deltahis graph can be used to predict the scattering angle of the electron beam passing through the ALPIDE sensor. The three ALPIDE sensors are focused to consider the scattering angle as in figure 6.7 (right). The angle of dispersion (θ) can be expanded by the difference of track position (Δx, and Δy) divided by the distance between the ALPIDE sensor (L). So, the scattering angle of electron on plane-*i* can be calculated by
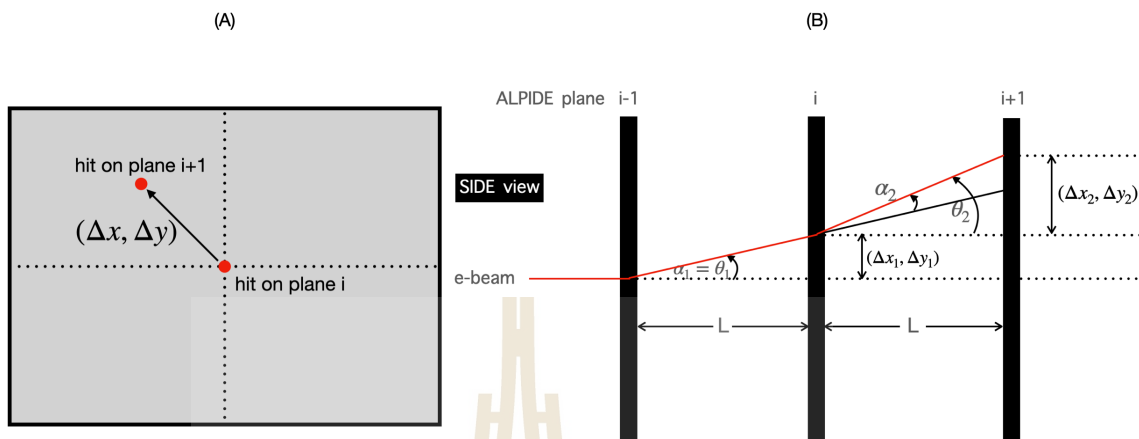
Figure 6.7 An electron track position which hit on ALPIDE sensor, the front view of track (a) and side view of track (b).
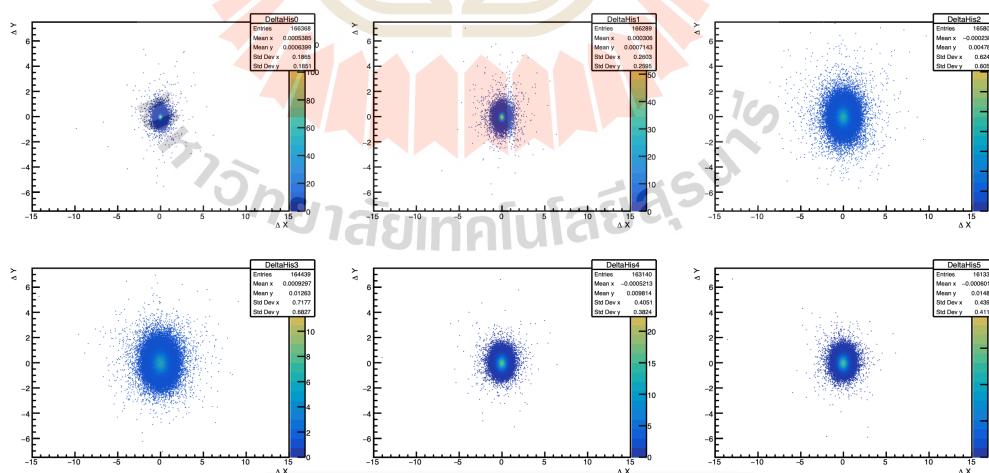

Figure 6.8 Distribution of the difference between the track position of the DUT plane with the other planes.

$$\alpha_i = \sqrt{[(tan^{-1}\frac{\Delta x_i}{L} - tan^{-1}\frac{\Delta x_{i-1}}{L})]^2 + [(tan^{-1}\frac{\Delta y_i}{L} - tan^{-1}\frac{\Delta y_{i-1}}{L})]^2} \qquad (6.1)$$

6.3 Comparison of the prediction with theoretical

The prediction of the scattering angle is discussed in the previous section. It can be calculated as in Eq. 6.1. So, we can predict the scattering angle of all-plane when the angle of the DUT plane was changed from 0, 10, 20, 30, and 40 degrees. Figure 6.9 shows the distribution of the scattering angle, the y-axis is the event number, and the x-axis is the scattering angle. The expected value of the scattering angle can be obtained after the distribution graph was fit by using Gumbel distribution. This work uses the expected value of the scattering angle to compare with the theory value.

The plot between the scattering angle (α) and the ALPIDE plane number is shown in figure 6.10, the line represents the scattering angle of 0 (black), 10 (red), 20 (green), 30 (blue), and 40 degrees (purple). The thick line represents the scattering value that can be calculated by using Eq. 2.8 as $\theta_0 = \frac{13.6}{\beta cp} z\sqrt{x/X_0}[1 + 0.038ln(x/X_0)]$ where the characteristic of the material is X_0. X_0 can be found by using an approximated formula (Eq. 2.9). The silicon properties are used to calculate X_0, which is 0.937 μm. Then X_0 is put back into Eq. 2.8 to find the angular dispersion. Especially, the velocity of the electron at SLRI is 0.9999869 times the speed of light. The charge of electron is 1. Energy is 1200 MeV. The thickness of ALPIDE sensor are varying between 50, 100, 150, 200, 250 and 300 μm .

For a DUT that is not rotated, the scattering angle of the first and second plans are around 0.0063 and 0.0092 degrees. The third plane has a scattering
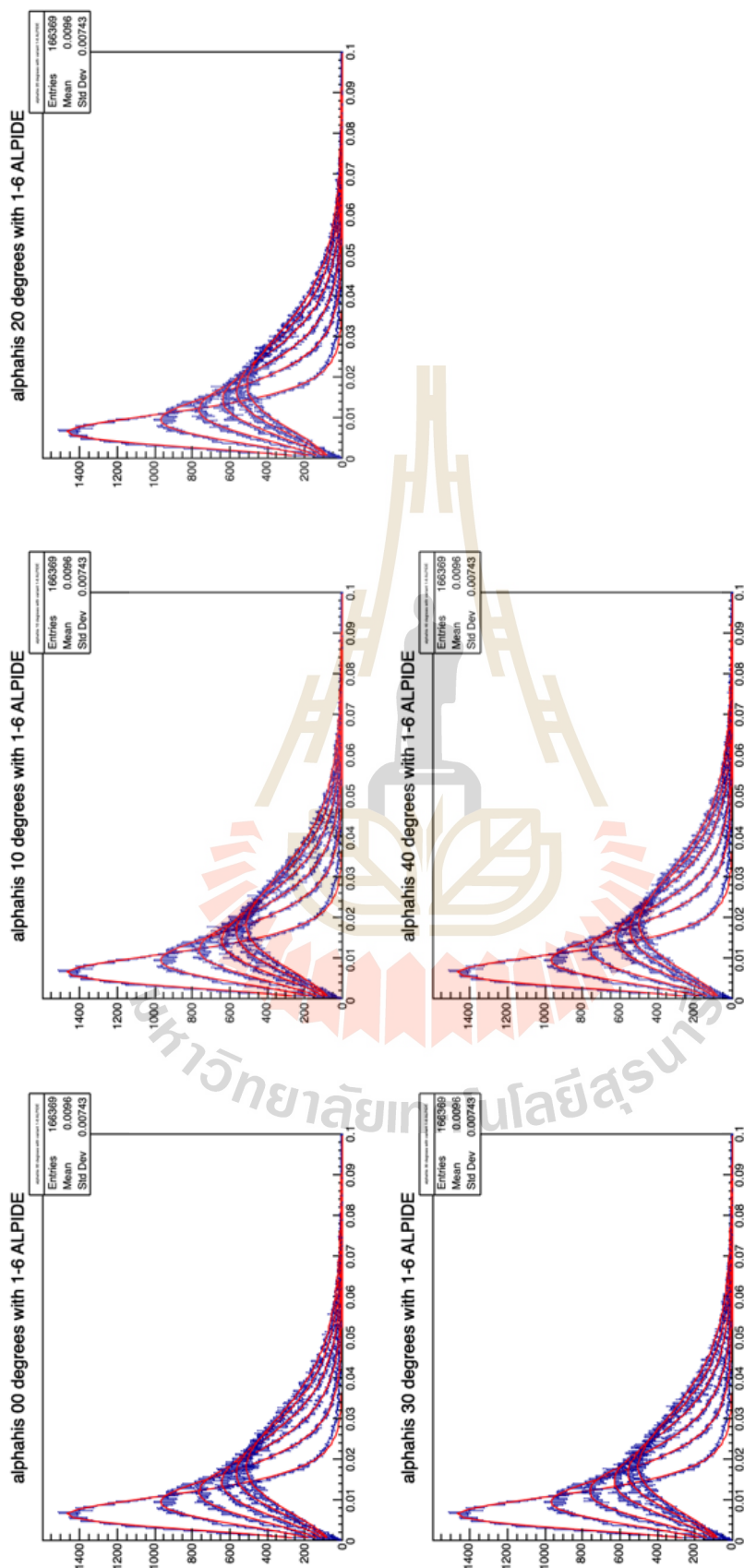
Figure 6.9 The histogram show the particle event distribution with the scattering angle. Each canvas is including 6 distributions, it show the distribution of 6 ALPIDE planes.
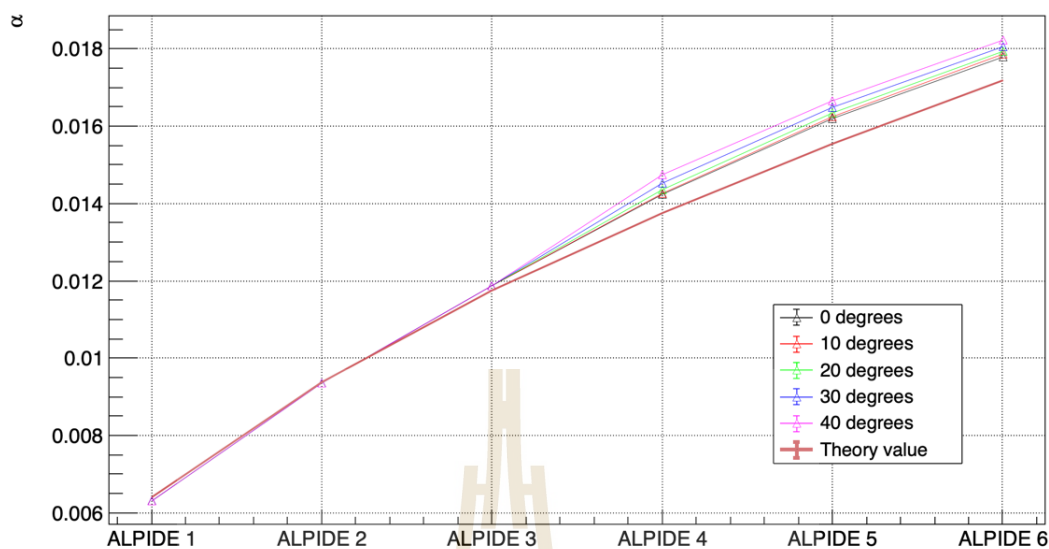
Figure 6.10 The plot between the scattering angle (α) with the ALPIDE plane number.

angle which is slightly greather than a theory prediction. The fourth, fifth and sixth planes have more value than a theory. For a rotated DUT case, the scattering angle (α) varies with the changing in DUT angle, α increases when DUT angle increase.

Summary

This work can predict the scattering angle of the electron which is under the condition of the new pixel sensor telescope. In the case of a rotated DUT, it is a result of the ALPIDE thickness. The ALPIDE thickness is 50 μm. When the DUT plane is rotated, its thickness increases. New thickness is equal to cosine of rotated angle times original thickness, see figure 6.11. An electron needs to pass through the sensor thickness longer than that of not rotated. It results in the increase of the scattering angle. For example, we can see the α value increases at ALPIDE 4 in figure 6.10.

In the case of a non-rotated DUT, this work compares the simulation value

with the theoretical value. The theoretical value is calculated by Eq. 2.8 by varying silicon thickness (other parameters are fixed). The simulation value is calculated with air between the ALPIDE plane (see in Appendix B.2). So, electrons slightly scatter when they traverse in air.
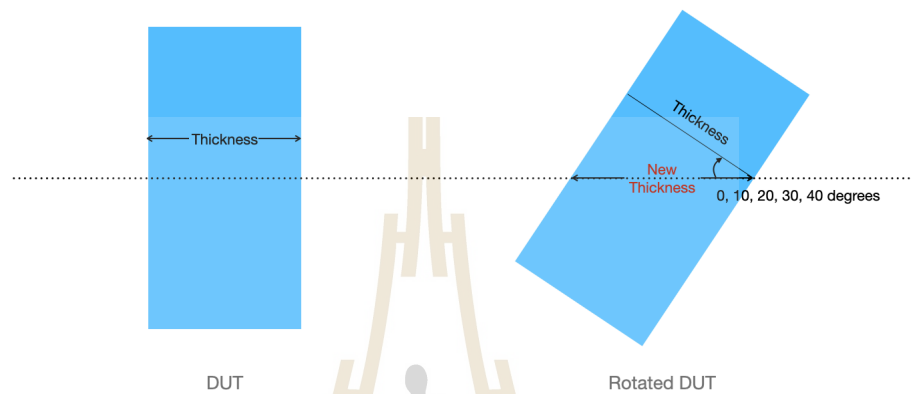

Figure 6.11 Thickness of DUT plane during original and rotated.

CHAPTER VII

CONCLUSIONS AND OUTLOOK

The ALICE team developed a simulation software for the test beam characterization for sensor prototypes of ITS2. It is called "a telescope optimizer", and used to specify the suitable boundary of the pixel sensor telescope for the test beam characterization. Additionally, the telescope optimizer predicted the particle trajectory. The optimal boundary conditions were being applied to the new pixel sensor telescope that was being constructed at the SLRI-BTF.

The upgraded ITS will be installed during the LS2 in 2021 at CERN Point2. For the original plan, the surface commissioning must be completed before April, 2020. Suranaree University of Technology has responsibility to support the manpower for the surface commissioning. The main duty was to the monitor and test a detector as a shifter for a total period of six months. The inner barrel has been tested 80% of total integrity and another 20% has been done for the outer barrel. The underground commissioning will be completed in the year 2021. However, after the World Health Organization announced Covid-19 is a pandemic in the early of 2020, the ITS2 installation was delayed at least 4-6 months. Currently, the installation is still ongoing.

Within this thesis, the upgrade of the pixel sensor telescope by using the electron beam at 1.2 GeV at the Synchrotron light research institute was studied. The simulation of the new pixel sensor telescope was done by using the G4beamline software and the ROOT was used as the analysis framework. The analysis result was used to predict the scattering angle of the new pixel sensor telescope, which is

equal to 0.0142 degrees in DUT of the non-rotated case. This work also shows the scattering angle prediction for the DUT rotated case. Moreover, the simulation result was compared with the calculation from the theory. For a non-rotated DUT case, the scattering angle of the upgrade of the pixel sensor telescope give a similar value to that of the theory calculation.

In conclusion, the result of this work shows that the G4beamline simulation can be used to predict the beam characterization. Moreover, this work also shows that ALPIDE sensor is a suitable for particle tracking, since it provides very low impact to the scattering angle, which gives better accuracy when we do the particle track reconstruction.
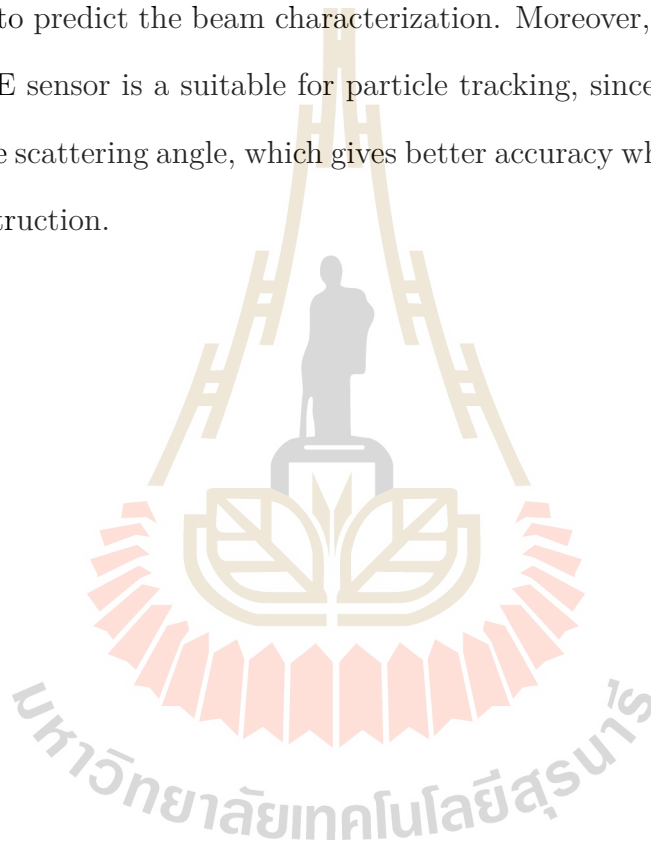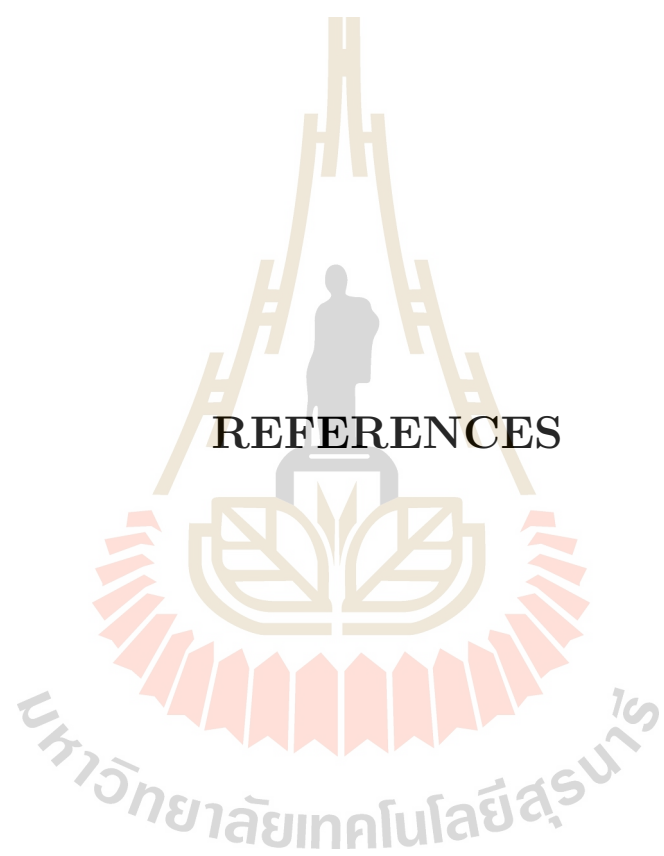
REFERENCES

REFERENCES

Aamodt, K., Quintana, A. A., Achenbach, R., Acounis, S., Adamová, D., Adler, C., Aggarwal, M., Agnese, F., Rinella, G. A., Ahammed, Z., Ahmad, A., Ahmad, N., Ahmad, S., Akindinov, A., Akishin, P., Aleksandrov, D., et al. (2008). The alice experiment at the cern lhc. **Journal of Instrumentation**. 3(08): S08002.

Abelev, B., Adam, J., Adamová, D., Aggarwal, M., Aglieri Rinella, G., Agnello, M., Agostinelli, A., Agrawal, N., Ahammed, Z., Ahmad, N., Ahmad Masoodi, A., Ahmed, I., Ahn, S., Ahn, S., Aimo, I., Aiola, S., et al. (2014). Technical design report for the upgrade of the alice inner tracking system. **Journal of Physics G: Nuclear and Particle Physics**. 41.

Agostinelli, S., Allison, J., Amako, K., Apostolakis, J., Araujo, H., Arce, P., Asai, M., Axen, D., Banerjee, S., Barrand, G., Behner, F., Bellagamba, L., Boudreau, J., Broglia, L., Brunengo, A., et al. (2003). Geant4–a simulation toolkit. **Nuclear Instrument Method A**. 506(3): 250-303.

Bakowski, M. and Gustafsson, U. (1998). Depletion region stopper for pn junction in silicon carbide. US Patent 5,801,836.

Brun, R. and Rademakers, F. (1997). Root—an object oriented data analysis framework. **Nuclear Instruments and Methods in Physics Research Section A: Accelerators, Spectrometers, Detectors and Associated Equipment**. 389(1-2): 81–86.

Cavicchioli, C., Chalmet, P., Giubilato, P., Hillemanns, H., Junique, A., Kugath-

asan, T., Mager, M., Tobon, C. M., Martinengo, P., Mattiazzo, S., Mugnier, H., Musa, L., Pantano, D., Rousset, J., and Reidt, F. (2014). Design and characterization of novel monolithic pixel sensors for the alice its upgrade. **Nuclear Instruments and Methods in Physics Research Section A: Accelerators, Spectrometers, Detectors and Associated Equipment**. 765: 177–182.

DESY collaboration (2013). Eutelescope, a generic pixel telescope data analysis framework. [Online]. Available: `http://eutelescope.web.cern.ch`.

Dorokhov, A., Bertolone, G., Baudot, J., Colledani, C., Claus, G., Degerli, Y., Masi, R. D., Deveaux, M., Dozière, G., Dulinski, W., Gélin, M., Goffe, M., Himmi, A., Hu-Guo, C., and Jaaskelainen, K. (2011). High resistivity cmos pixel sensors and their application to the star pxl detector. **Nuclear Instruments and Methods in Physics Research Section A: Accelerators, Spectrometers, Detectors and Associated Equipment**. 650(1): 174-177.

Keil, M. (2015). Upgrade of the ALICE inner tracking system. **Journal of Instrumentation**. 10(03): C03012–C03012.

Kittimanapun, K., Chanlek, N., Cheedket, S., Juntong, N., Klysubun, P., Krainara, S., Sittisard, K., and Supajeerapan, S. (2016). SLRI Beam Test Facility Development Project. In **7th International Particle Accelerator Conference**. WEPMY002: 2538.

Kittimanapun, K., Chanlek, N., Klysubun, P., Kobdaj, C., Lakrathok, A., Laojamnongwong, N., Mager, M., and Musa, L. (2019). Development of the slri beam test facility for characterization of monolithic active pixel sensors.

Nuclear Instruments and Methods in Physics Research Section A: Accelerators, Spectrometers, Detectors and Associated Equipment. 930: 105–111.

Kittimanapun, K., Chanlek, N., Klysubun, P., Krainara, S., and Supajeerapan, S. (2017). Improvement of Electron Intensity Reduction System at SLRI Beam Test Facility. In **8th International Particle Accelerator Conference**. MOPIK015: 528.

Lazanu, I., Lazanu, S., Biggeri, U., Borchi, E., and Bruzzi, M. (1997). Non-ionising energy loss of pions in thin silicon samples. **Nuclear Instruments and Methods in Physics Research Section A: Accelerators, Spectrometers, Detectors and Associated Equipment**. 388(3): 370–374.

Mager, M. (2016). ALPIDE, the Monolithic Active Pixel Sensor for the ALICE ITS upgrade. **Nuclear Instrumentsand Methods in Physics Research A**. 824: 434.

Meroli, S. (2015). In-depth study of phenomena characterizing the passage of ionizing particles through semiconductor layers [Online]. Available: `https://meroli.web.cern.ch/files/the_bible_of_the_interactions.pdf`.

Moore, G. D. and Teaney, D. (2005). How much do heavy quarks thermalize in a heavy ion collision? **Physical Review C**. 71(6): 064904.

Morgan Jr, S. and Eby, P. (1973). Corrections to the bethe-bloch formula for average ionization energy loss of relativistic heavy nuclei close collisions. **Nuclear Instruments and Methods**. 106(3): 429–435.

Musa, L. (2012). Conceptual Design Report for the Upgrade of the ALICE ITS. [Online]. Available: `https://cds.cern.ch/record/1431539`.

Perrey, H. (2014). Eudaq and eutelescope software frameworks for testbeam data acquisition and analysis. **Technology and Instrumentation in Particle Physics**. 353.

Ranjan, A. and Ravishankar, V. (2010). Introduction to quark-gluon plasma. **Indian Journal of Physics**. 84(1): 11-40.

Roberts, T., Beard, K., Huang, D., Ahmed, S., Kaplan, D., and Spentzouris, L. (2008). G4beamline particle tracking in matter-dominated beam lines, conf. **Proceeding Conference**. 806233.

Satz, H. (2011). The Quark-Gluon Plasma: A Short Introduction. **Nuclear Physics A**. 862-863: 4-12.

Scandale, W., Arduini, G., Butcher, M., Cerutti, F., Garattini, M., Gilardoni, S., Lechner, A., Losito, R., Masi, A., Mirarchi, D., et al. (2017). Measurements of multiple scattering of high energy protons in bent silicon crystals. **Nuclear Instruments and Methods in Physics Research Section B: Beam Interactions with Materials and Atoms**. 402: 291–295.

Tsai, Y.-S. (1974). Pair production and bremsstrahlung of charged leptons. **Reviews of Modern Physics**. 46(4): 815.

Williams, B. (1977). *Compton scattering: the investigation of electron momentum distributions.* New York : McGraw-Hill International.
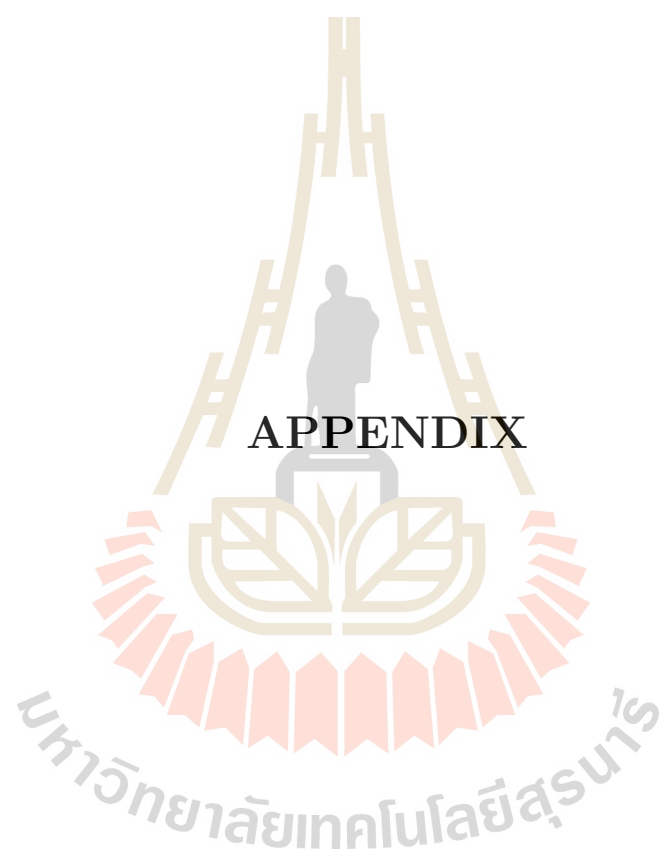
APPENDIX

APPENDIX

ADDITIONAL ANALYSIS FIGURES AND INFORMATION

The correlation graph The correlation plot shows the relation between the electron track on the plane i and plane $i+1$. The G4beamline simulation provides the correlation plots for all ALPIDE planes. Figure 1 shows the correlation plot in x-position via the changes of DUT angle. Figure 2 shows the correlation plot in y-position via the changes of DUT angle.

Scattering angle This section shows the plot between the scattering angle in the case of a non-rotated DUT case comparing with the theoretical values. For this case, the pixel sensor telescope was tested in a vacuum. So, this condition is used to do the G4beamline simulation. The result is plotted as a figure 3, the x-axis is the scattering angle in degrees unit, and the y-axis is the ALPIDE plane. The simulation gives us almost the same value as that of the theory. Therefore, this graphs prove that we can use the conditions of this work to do the simulation for sensor characterization.
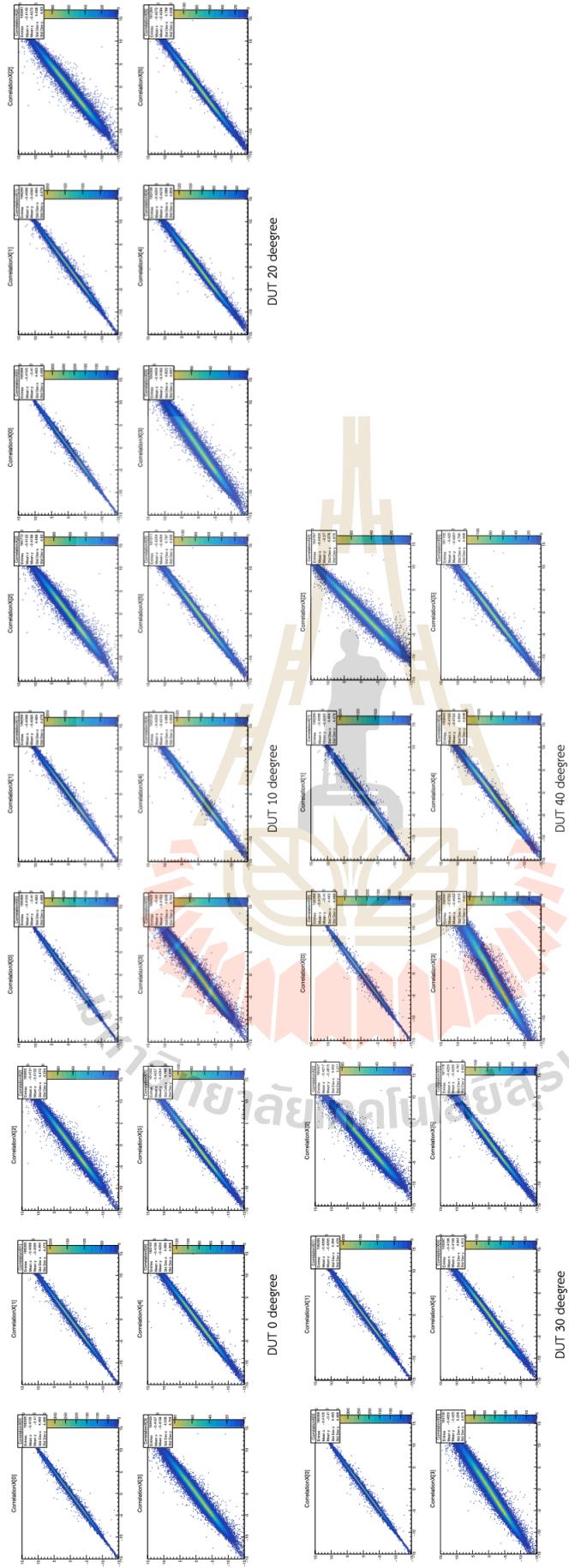
Figure 1 The correlation plot in the x-direction via the changes DUT angle. Canvas [0] represent the track position between the first and second plane. Canvas [1], [2], [3], [4] and [5] represent the track position between the second and third plane, third and fourth, fourth and fifth, fifth and sixth respectively.
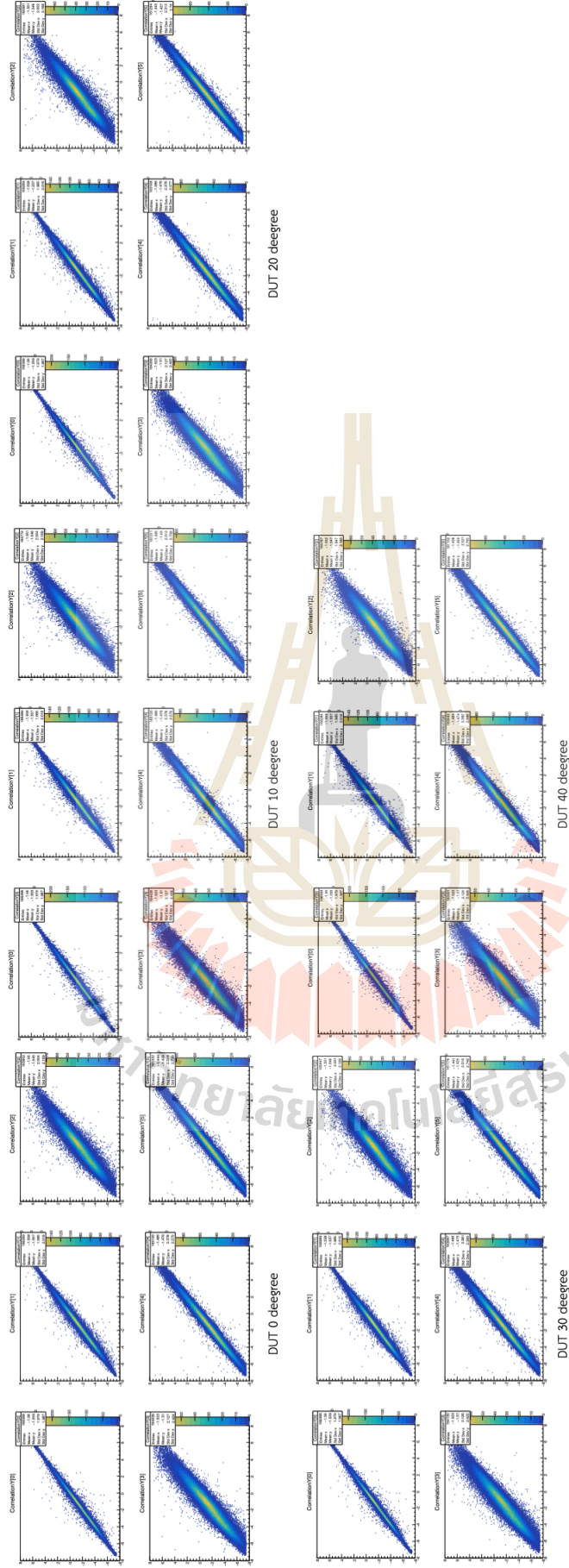
Figure 2 The correlation plot in the y-direction via the changes DUT angle. Canvas [0] represent the track position between the first and second plane. Canvas [1], [2], [3], [4] and [5] represent the track position between the second and third plane, third and fourth, fourth and fifth, fifth and sixth respectively.
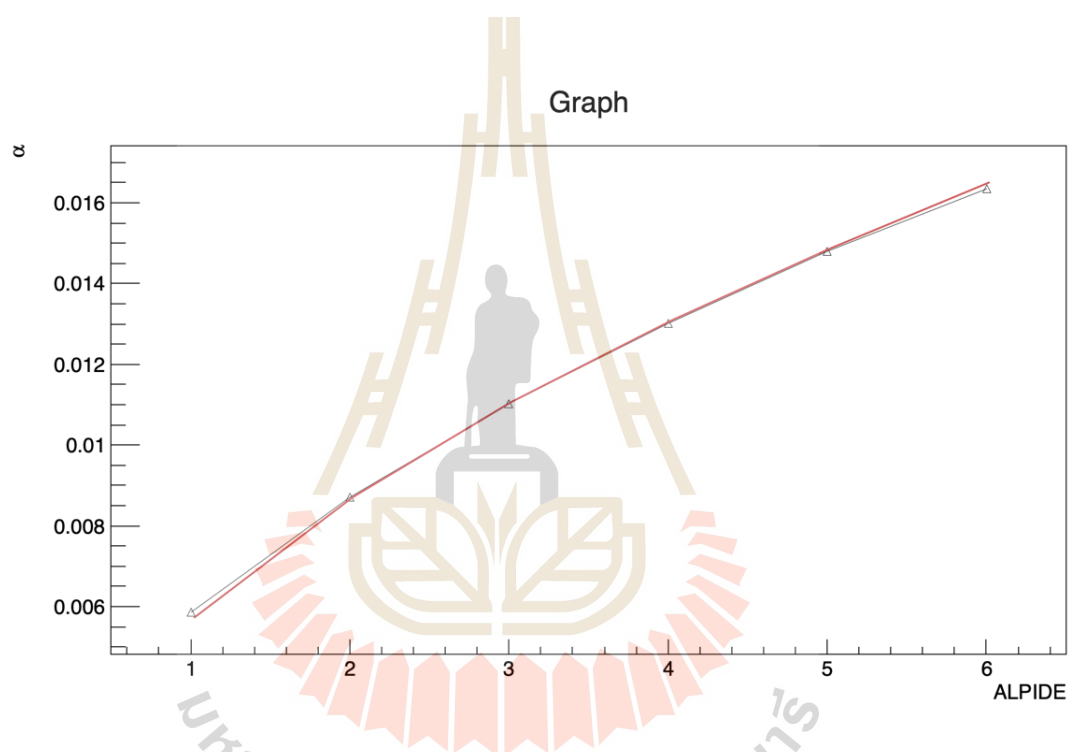
Figure 3 The plot between the scattering angle (α) with the ALPIDE plane number

CURRICULUM VITAE

NAME: Jetnipit Kaewjai   **GENDER**: Male

NATIONALITY: Thai   **DATE OF BIRTH**: Jan 13, 1995

E-MAIL: jetnipit.jaii@gmail.com

EDUCATIONS:

- 2008 - 2013, High School, Yasothon Pittayakom School, Thailand
- 2013 - 2016, Bachelor of Science, School of Physics, Institute of Science, Suranaree University of Technology, Thailand
- 2016 - 2019, Masterof Science, School of Physics, Institute of Science, Thailand

PUBLICATIONS

J. Kaewjai, C. Kobdaj and K. Kittimanapun (2019), Upgrade of pixel sensor telescope for the characterization of ALPIDE sensor, Journal of Physics: Conference Series, Volume 1380, doi: 10.1088/1742-6596/1380/1/012126.